Summer 7-10-2017

Statistical Topological Approach Using Wave-Chaos for Electromagnetic Effects (STUWEE)

Ghadeh M. Hadi
University of New Mexico - Main Campus

Ghadeh M. Hadi
Candidate

Electrical and Computer Engineering
Department

This dissertation is approved, and it is acceptable in quality and form for publication:

Approved by the Dissertation Committee:

Dr. Edl Schamiloglu , Chairperson

Dr. Sameer Hemmady

Dr. Zhen Peng

Dr. Salvador Portillo

Dr. Ylva Pihlstrom

Statistical Topological Approach Using Wave-Chaos for Electromagnetic Effects (STUWEE)

By

Ghadeh M. Hadi

B.S., Computer Engineering, University of New Mexico, 2010

M.S., Computer Engineering, University of New Mexico, 2012

Ph.D., Engineering, University of New Mexico, 2017

DISSERTATION

Submitted in partial fulfillment of the

Requirements for the Degree of

Doctor of Philosophy

Engineering

The University of New Mexico,

Albuquerque NM 87131, USA

July 2017

STATISTICAL TOPOLOGICAL APPROACH USING WAVE-CHAOS FOR ELECTROMAGNETIC EFFECTS (STUWEE)

By

Ghadeh M. Hadi

B.S., Computer Engineering, University of New Mexico, 2010

M.S., Computer Engineering, University of New Mexico, 2012

Ph.D., Engineering, University of New Mexico, 2017

ABSTRACT

Predicting the nature of the scattering of short wavelength waves in random interconnected networks of large complicated enclosures is routinely encountered in diverse fields such as acoustics, wireless communications, and electromagnetic compatibility engineering. The Random Coupling Model (RCM), based on wave-chaos, is a statistical model describing the scattering of short wavelength electromagnetic waves in large complicated (chaotic) enclosures. The Baum-Liu-Tesche (BLT) electromagnetic topology formulation is a hierarchical framework based on the multiconductor transmission line (MTL) model for describing the flow of energy between different nodes on a network of MTL segments, originally developed to study the coupling of electromagnetic waves to aircraft cable bundles. In this research, we fuse the RCM with the BLT electromagnetic topology to create the *"Statistical Topological Approach Using Wave-chaos for Electromagnetic Effects"* (STUWEE) tool for predicting the statistics of the scattering of short wavelength electromagnetic waves in random interconnected networks of chaotic enclosures. In this Dissertation, I provide experimental results demonstrating the

existence of wave-chaotic fluctuations in quasi-2D mode-stirred chambers (MSCs), in accordance with the RCM, and then show how these fluctuations are affected when considering random interconnections of MSCs using the BLT topology model. This work uses the BLT electromagnetic topology model to break down the networked cavities and the RCM to study statistics within each cavity. Experimental measurements have validated the fusing of the RCM with the BLT electromagnetic topology model for this application.

DEDICATION

Dedicated to my Parents,

Iqbal and Mustafa Hadi.

and my Siblings

Ali, Qamar, Hussain, Muhamad, Iraq and Fatemah

ACKNOWLEDGEMENTS

I am truly grateful to Professor Schamiloglu for giving me the opportunity to work on cutting-edge technology, and I am also grateful for his vital support, patient guidance, positive attitude and continual encouragement during my time as his Ph.D. student.

I want to thank Dr. Sameer Hemmady for all that he taught me, his patience with me in the last four years, and his help in solving the problems in my research.

I would like to thank all my colleagues, specifically Rusmir Bilalic and Joe Chen, for their moral support and encouragement.

I would like to thank Dr. Salvador Portillo, Dr. Zhen Peng, Dr. Yang Shao and Shen Lin for collaborating with me.

Finally, I would like to thank my family, friends, all my professors at UNM, and all the amazing people in my life; I attribute my accomplishments to all of them.

The research described in this Dissertation was sponsored by ONR CDEW Grant N00014-14-1-0794 (Ryan Hoffman and Peter Morrison, Program Officers) and AFOSR COE Grant FA9550-15-1-0171 (Jason Marshall, Program Officer).

TABLE OF CONTENTS

List of Figures

Chapter 1: Introduction

Electromagnetic fields exist wherever electrical power is generated, transmitted, or received. Electromagnetic fields can also be produced in strong bursts of short wavelength energy caused by a rapid acceleration of charged particles in a process that is referred to as the Electromagnetic Pulse (EMP). Such a pulse's origin may be a natural event or man-made, and can occur as a radiated electric or magnetic field, or a conducted electric current, depending on the nature of the source.

Our environment is polluted with electromagnetic radiation emitted from various sources, either naturally occurring or man-made. Natural occurrences originate from such phenomena as lightning, electrostatic discharge (ESD), geomagnetic storms, and so on. Man-made sources can be a consequence of the ubiquitous presence of electromagnetic waves in our environment from such sources as wireless data services, radar, and nonnuclear electromagnetic weapons (also referred to as high power microwaves – HPM, or intentional electromagnetic interference – IEMI).

In the 1960's, the testing of a nuclear weapon in the atmosphere produced an electromagnetic pulse that caused RF upset in electronic systems. The nuclear detonation created an EMP with a frequency spectrum in the MHz range. Later, HPM weapons were made to produce a similar EMP-like effect, albeit in shorter pulses, as narrowband or ultra-wideband sources with their frequency spectrum ranging from approximately 300 MHz-10 GHz and even higher. This is the frequency range of interest in this research. EMP or IEMI can couple into closed enclosures (or cavities); this interference can be disruptive or damaging to any electronic equipment inside the enclosures.

The short wavelength electromagnetic radiation couples into a cavity through any apertures or gaps between panels of an enclosure; these openings act as slot antennas, helping the electromagnetic energy to enter and resonate within the enclosure, causing the enclosure to act as a microwave cavity. Therefore, there is an urgent need to study the effects of short wavelength electromagnetic radiation on cavities to be able to protect critical electronic equipment inside multiple arbitrarily interconnected enclosures and, hence, the motivation for this research.

1.1 Statistical Approach

Understanding the interaction of short wavelength electromagnetic energy with arbitrarily interconnected complicated cavities is of interest in several branches of physics and engineering. The coupling properties of enclosures depend on the details of the shape of the enclosures, the size of the enclosures, the structures of the apertures when there are incoming and outgoing waves, and the frequency of the radiation. The coupling properties also depend on the internal geometry within the enclosures which are extremely sensitive to small changes in the frequency of the electromagnetic radiation, shape of the enclosure, and the orientation of the components inside. A slight change, such as a simple wire bend, can result in acutely different field patterns that require new detailed knowledge that will provide no information about the previous nearly identical configuration [1].

3D numerical analysis using computational electromagnetics has been facilitated by significant advances in computer technology. However, when the wavelength of the electromagnetic radiation becomes much smaller than the enclosure size of the target system, the computational time and CPU resources required for such simulations can be costly. In the limit of short wavelength, the electromagnetic field quantities within the enclosure are very sensitive to the enclosure shape, the internal object positions, the incident radiation frequency, and the geometry

of coupling ports [1]. Furthermore, precise knowledge of all the boundary conditions would also be required to accurately perform a deterministic calculation, which is a near impossible feat. Therefore, a statistical approach is required that treats the bounded electromagnetic field quantities as random variables and the nature of their fluctuations is characterized by suitable probability density functions (PDFs).

In this research, we want to develop a predictive capability that fuses the random coupling model (RCM) with the electromagnetic topology model of Baum-Liu-Tesche, a statistical model that predicts the scattering wave fluctuation in a single volume, and a transmission line topology that studies the energy flow through multiple volumes connected by transmission lines. Combining BLT and RCM will enable us to predict the statistics of the scattering of short-wavelength electromagnetic waves in randomly interconnected networks of chaotic enclosures.

1.2 Random Coupling Model (RCM)

The Random Coupling Model (RCM) is based on Random Matrix Theory (RMT) of wave-chaos. It is a statistical model describing the scattering of short wavelength electromagnetic waves in large wave-chaotic enclosures. The RCM makes statistical predictions of induced voltages and currents for objects and components contained inside ray-chaotic enclosures subjected to electromagnetic fields. The RCM states that all wave-chaotic systems, regardless of their geometric complexities, possess universal statistical properties in their wave-scattering fluctuation characteristics that can be described by the statistical properties of ensembles of large random matrices; however, there are some system-specific, non-universal aspects of the problem that are quantified by means of the complex radiation impedance of the coupling ports in the cavity. A coupling port is any way in which an electromagnetic wave can enter or exit the

enclosure, or be absorbed within the enclosure. Fig. 1.1 is a schematic overview description of the RCM.

In the RCM, chaotic ray trajectories are assumed. Unlike the case in traditional chaotic dynamics where the governing equation is nonlinear and the time-development of the system is highly sensitive to initial conditions, in the RCM the system is linear. However, the trajectories of two adjacent rays diverge exponentially due to the geometry of the cavity. Hence the notion of wave-chaos.

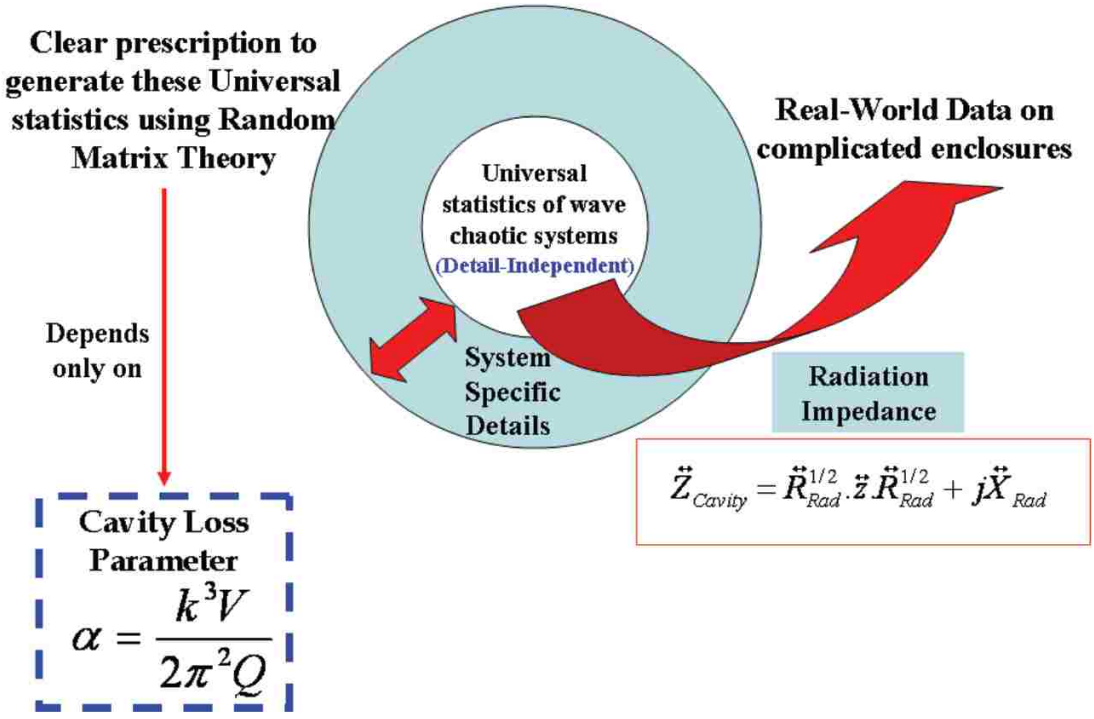

Fig. 1.1. Schematic overview of the RCM [1].

1.3 The Baum-Liu-Tesche (BLT) Electromagnetic Topology Model

The BLT electromagnetic topology model was developed in 1986 to understand RF penetration into large and complicated enclosures such as aircrafts, ships, buildings, etc., and then onto cable bundles. This effort was motivated by the problem of Nuclear EMP (NEMP) coupling onto wire

bundles in aircraft. NEMP is a consequence of the atmospheric detonation of a nuclear weapon. The BLT electromagnetic topology model involves the division of a large complicated electromagnetic system into smaller subsystems represented as junctions connected to each other using transmission lines to establish an environment that mimics that of large enclosures. The BLT electromagnetic topology model is a hierarchical framework based on the MTL model for describing the flow of energy between different nodes on a network of MTL segments.

After a large volume is topologically broken down into smaller sub-volumes, the electromagnetic interaction within it is then represented by the BLT equation:

$$\left\{\vec{\vec{I}} - \vec{\vec{S}} \cdot \vec{\vec{\Gamma}}\right\} \cdot [W(0)] = \vec{\vec{S}} \cdot [W_S]. \tag{1.1}$$

Fig. 1.2. presents a drawing showing the use of the electromagnetic topological approach to sub-divide a large system (an airplane) into smaller subsystems.

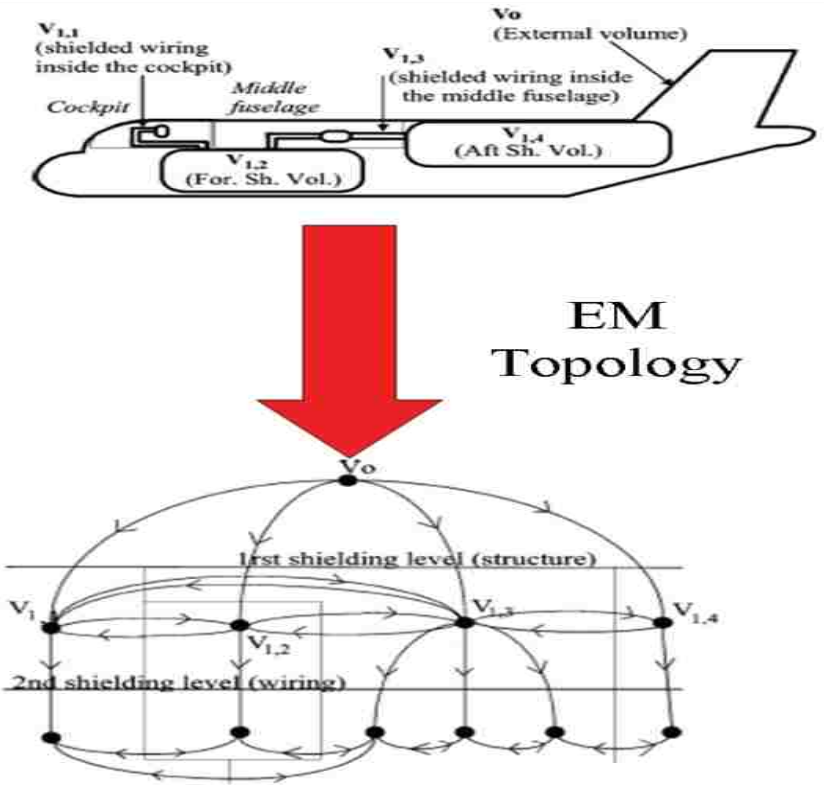

Fig. 1.2. Schematic illustrating the electromagnetic topological approach subdividing a system into smaller subsystems [2].

1.4 Fusing BLT with RCM

In this research, we fuse the RCM with the BLT electromagnetic topology model to predict the statistics of the scattering of short wavelength electromagnetic waves in randomly interconnected networks of chaotic enclosures. In this Dissertation, we present experimental results demonstrating the existence of wave-chaotic fluctuations in a large 3D mode stirred chamber (MSC) and in five quasi-2D MSCs, in accordance with the RCM. The networked quasi-2D cavities are used to develop a computational framework that fuses the RCM with the BLT electromagnetic topology model.

Fusing the RCM with the BLT electromagnetic topology will enable a rapid assessment of the electromagnetic coupling within large complicated systems, and their possible impact on sensitive electronics. This work uses the BLT electromagnetic topology to break down the network of cavities and the RCM to study the statistics within each cavity.

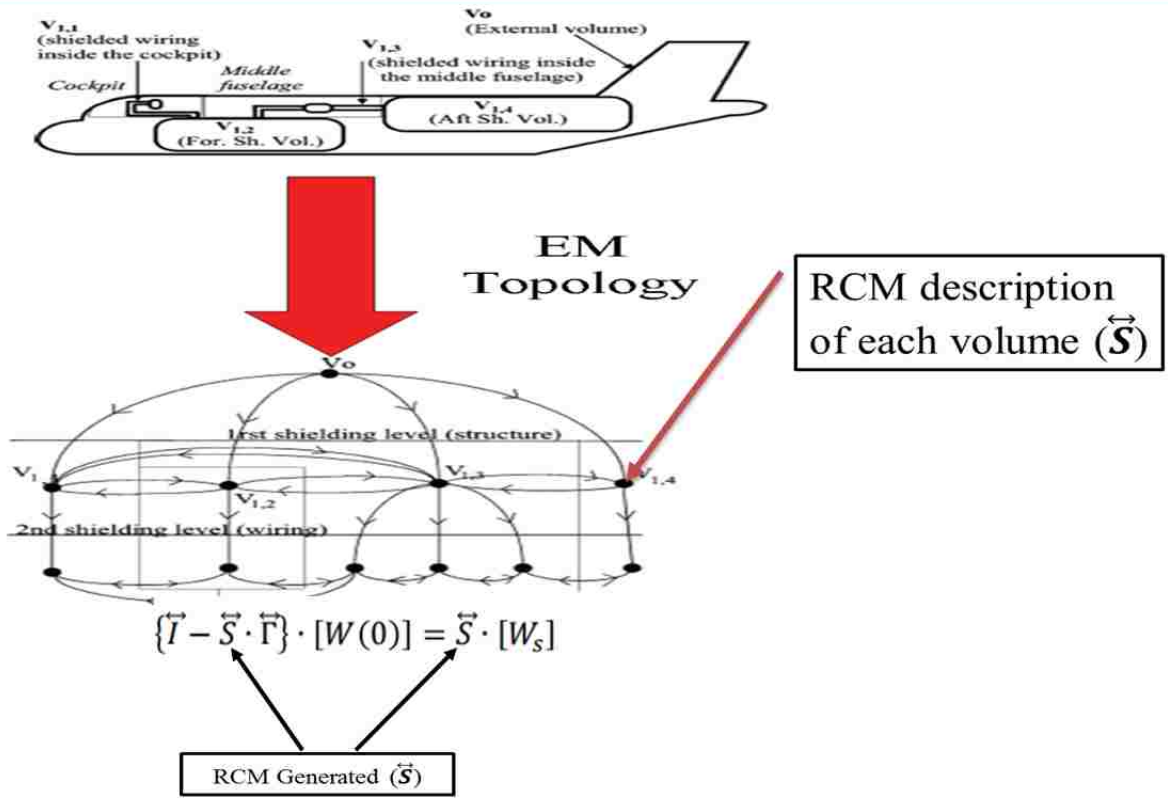

Fig. 1.3. Fusing the BLT electromagnetic topology model with the RCM.

1.5 Organization of this Dissertation

The research described in this Dissertation seeks to experimentally validate the fusing of the RCM with the BLT electromagnetic technology. The remainder of this Dissertation is organized as follows:

- Chapter 2 presents an overview of the RCM and experimental results from quasi-2D cavities that verify their wave-chaotic nature.

- Chapter 3 provides an overview of the BLT electromagnetic topology model. We experimentally construct a BLT network that mimics the construction of a facility to test our statistical approach validation when comparing BLT topology theoretically and experimentally.
- In Chapter 4 we study the transition from deterministic to wave-chaotic behavior in a large 3D chaotic cavity.
- Finally, Chapter 5 presents a summary of the results discussed in this Dissertation and suggests the scope of future work.

Chapter 2: Random Coupling Model

The RCM, introduced by the "chaos group" at the University of Maryland in the early 2000's, focuses on the problem of statistically modeling the scattering of short wavelength electromagnetic waves inside irregularly shaped enclosures connected to an external RF source by one or multiple ports. The RCM is an approach based on RMT and wave-chaos to predict the induced voltages and currents for objects and components inside complicated enclosures when subjected to electromagnetic fields. This is achieved by generating a large ensemble of the cavity impedance or scattering parameters through a Monte Carlo (MC) simulation and providing information on the cavity loss parameter and the complex radiation impedance of the coupling ports.

This study focuses on the limit of electromagnetic waves of high-frequency coupling into metallic enclosures of irregular shapes where the wavelengths are very short compared to the perimeter of a cavity which causes the waves to go under specular reflection. Therefore, the RCM provides solutions for linear wave equations that can be described by ray-chaotic trajectories.

2.1 Radiation Impedance Normalization of One- and Multi-Port Systems

The RCM characterizes the fluctuations in the impedance and scattering matrices for a ray-chaotic enclosure coupled to N ports. The cavity scattering matrix $\overleftrightarrow{\mathrm{S}}$ models the scattering waves in the enclosure in terms of a matrix of N×N complex values. $\overleftrightarrow{\mathrm{S}}$ is the amplitude of N outgoing scattered waves ($\tilde{b}$) for N incoming scattered waves ($\tilde{a}$) at the location of each port (i.e. $\tilde{b}= \overleftrightarrow{S}\tilde{a}$). The impedance matrix $\overleftrightarrow{\mathrm{Z}}$ relates the complex voltages V at the N driving ports to the complex currents I at the N ports through

$$\tilde{V} = \overleftrightarrow{Z}\tilde{I}. \tag{2.1}$$

The matrices $\overleftrightarrow{S}$ and $\overleftrightarrow{Z}$ are strongly varying functions of frequency, and are related through the bilinear transformation,

$$\overleftrightarrow{Z} = \overleftrightarrow{Z}_0\left(\overleftrightarrow{1} + \overleftrightarrow{S}\right)/\left(\overleftrightarrow{1} - \overleftrightarrow{S}\right) \text{ for one-port, and} \tag{2.2}$$

$$\overleftrightarrow{Z} = \overleftrightarrow{Z}_0^{1/2}\left(\overleftrightarrow{1} + \overleftrightarrow{S}\right)\left(\overleftrightarrow{1} - \overleftrightarrow{S}\right)\overleftrightarrow{Z}_0^{1/2} \text{ for multiple-ports,} \tag{2.3}$$

where $\overleftrightarrow{Z}_0$ is an N×N non-complex diagonal matrix whose elements are the characteristic impedances of the transmission line input channels at the N driving ports. $\overleftrightarrow{Z}$ has a mean part given by the radiation impedance

$$\overleftrightarrow{Z}_{\text{rad}} = \langle\overleftrightarrow{Z}\rangle. \tag{2.4}$$

According to the RCM, for a wave-chaotic cavity coupled with N ports, the statistical impedance matrix consists of the radiation impedance matrix $\overleftrightarrow{Z}_{\text{rad}}$ and the normalized impedance matrix $\overleftrightarrow{z}$, as shown in Eq. (2.5) [1]

$$\overleftrightarrow{Z} = \text{i Im}\left[\overleftrightarrow{Z}_{\text{rad}}\right] + \left(\text{Re}\left[\overleftrightarrow{Z}_{\text{rad}}\right]\right)^{1/2}\overleftrightarrow{z}\left(\text{Re}\left[\overleftrightarrow{Z}_{\text{rad}}\right]\right)^{1/2}. \tag{2.5}$$

The radiation impedance $\overleftrightarrow{Z}_{\text{rad}}$ is the impedance that can be obtained from the radiation scattering matrix $\overleftrightarrow{S}_{\text{rad}}$ through Eq. (2.6)

$$\overleftrightarrow{Z}_{\text{rad}} = \overleftrightarrow{Z}_0\left(\overleftrightarrow{I} + \overleftrightarrow{S}_{\text{rad}}\right)/\left(\overleftrightarrow{I} + \overleftrightarrow{S}_{\text{rad}}\right), \text{ for one-port, and} \tag{2.6}$$

$$\overleftrightarrow{Z}_{\text{rad}} = \overleftrightarrow{Z}_0^{1/2}\left(\overleftrightarrow{I} + \overleftrightarrow{S}_{\text{rad}}\right)\left(\overleftrightarrow{1} - \overleftrightarrow{S}_{\text{rad}}\right)^{-1}\overleftrightarrow{Z}_0^{1/2}, \text{ for multiple-ports.} \tag{2.7}$$

Once we obtain the radiation impedance we can then obtain the normalized impedance matrix $\overleftrightarrow{z}$ and the normalized scattering matrix $\overleftrightarrow{s}$ via

$$\overleftrightarrow{z} = \left(\overleftrightarrow{Z} - \text{iIm}\left[\overleftrightarrow{Z}_{\text{rad}}\right]\right)/\left(\text{Re}\left[\overleftrightarrow{Z}_{\text{rad}}\right]\right), \text{ for one-port, and} \tag{2.8}$$

$$\overleftrightarrow{z} = \left(\mathrm{Re}\left[\overleftrightarrow{Z}_{rad}\right]^{-1/2}\left(\overleftrightarrow{Z} - i\mathrm{Im}\left[\overleftrightarrow{Z}_{rad}\right]\right)\left(\mathrm{Re}\left[\overleftrightarrow{Z}_{rad}\right]\right)^{-1/2}\right), \text{ for multiple-ports.} \quad (2.9)$$

Finally, the normalized scattering parameter is given by

$$\overleftrightarrow{s} = \left(\overleftrightarrow{z} - \overleftrightarrow{1}\right)\left(\overleftrightarrow{z} + \overleftrightarrow{1}\right)^{-1}. \quad (2.10)$$

2.2 Generating Normalized Impedance Matrices from Monte Carlo Simulations

The normalized impedance $\overleftrightarrow{z}$ only depends on the loss parameter α, which can be defined as

$$\alpha = \frac{K^2}{\Delta k_n^2 Q} \quad \text{for 2D cavities, and} \quad (2.11)$$

$$\alpha = \frac{K^3}{\Delta k_n^3 Q} \quad \text{for 3D cavities.} \quad (2.12)$$

As described in his Ph.D. Thesis, Hemmady [1] derived the normalized impedance from RMT and the random plane wave hypothesis, which gives the formula for $\overleftrightarrow{z}$ for the multi-port case:

$$\overleftrightarrow{Z} = \frac{-j}{\pi}\sum_{n=1}^{M}\frac{\overleftrightarrow{w}_N\overleftrightarrow{w}_N^T}{k^2 - k_n^2/\Delta k_n^2 - j\alpha}, \quad (2.13)$$

where $k = 2\pi f/c$ is the wavenumber corresponding to the incoming frequency, k_n is the wavenumber corresponding to a cavity eigenvalue, Δk_n^2 is the mean spacing of adjacent eigenvalues, $\overleftrightarrow{w}_N$ is an N-dimensional Gaussian random column vector with zero mean and its covariance matrix is the identity matrix, and α is the dimensionless cavity loss parameter. More details on the derivation of $\overleftrightarrow{z}$ using the random plane wave hypothesis for the one- and multiple-port cases is given in Ref. [3] and [4], respectively. Eq. (2.13) can then be evaluated numerically using MATLAB. More details on MC simulations can be found in [1].

2.3 Experimental Setup for 2D Cavities for RCM Verification

We fabricated 5 quasi-2D aluminum cavities. When we describe an enclosure or a cavity as a quasi-2D wave-chaotic cavity, we require that its maximum frequency does not exceed c/2d, where c is the speed of light and d is the height of the resonator [5]; in other words, the depth of the cavity is much smaller than the wavelength of electromagnetic radiation. The depth of our quasi-2D cavities does not exceed 8 mm.

Each cavity acts as a reverberation chamber with a mode stirrer at each corner and in the middle to prevent the unwanted localization of electromagnetic fields (Fig. 2.1). Along with these cavities, we fabricated aluminum inserts of different shapes that alter the internal boundary condition within each cavity. Fig. 2.1 shows the different internal configurations for a set of quasi-2D cavities obtained by using metal inserts to achieve a bow tie shape, a semi-circular shape, an elliptical shape, and a bi-elliptical shape. Fig. 2.1 also shows the mode stirrers (shaped like crosses) inside each cavity. Each rotation of the mode stirrer yields a different electromagnetic field configuration inside the cavities. Each mode stirrer is connected to a stepper motor (NI NEMA 23) (Fig. 2.2) for automation using the Arduino board (Fig. 2.3) for control.

a. Semi-circularly-shaped inserts.

b. Bi-elliptically-shaped insert.

c. Bow tie-shaped insert.

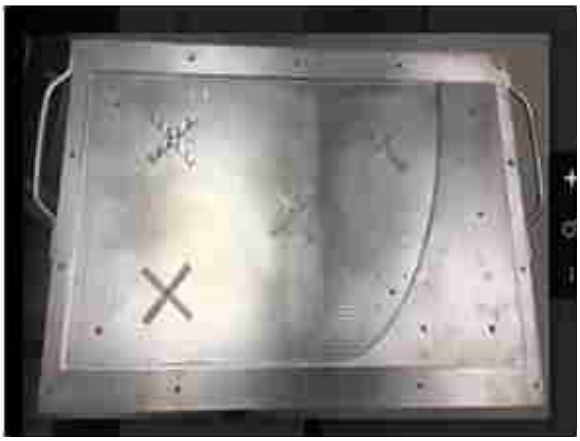

d. Elliptically-shaped insert.

Fig. 2.1. Photographs showing the experimental setup of multiple (a.-d.) quasi-2D wave-chaotic cavities with different geometry inserts.

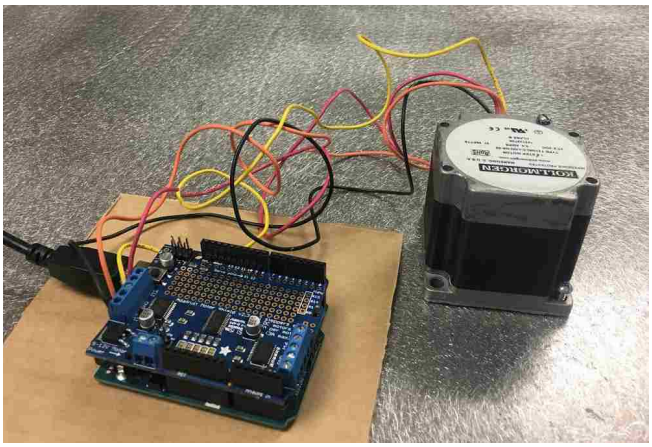

Fig. 2.2. Photograph of a stepper motor connected to a mode stirrer and controlled by an Arduino board.

The MATLAB code instructs the Arduino board to rotate the mode stirrers incrementally in 200 steps to yield a very large data set from the vector network analyzer (Keysight PNA-X N5247A) at each rotation of the mode stirrers. At each increment of rotation, we precisely extract 100001 points of complex scattering parameters as a function of frequency; the frequency range we work in is 50 MHz to 12 GHz, selected to study the transition from the deterministic regime to the

wave-chaotic regime. Therefore, we can generate a large statistical ensemble of cavity scattering matrices $\overleftrightarrow{S}$ to permit the study of electromagnetic penetration into each cavity.

Each 2D cavity's covering lid has 5 different antenna locations (Fig. 2.3). Depending on the shape we insert inside the cavity, some of these locations will not be available to use; using the available antenna locations, the cavity is then driven by one, two, or three SMA ports, Fig. 2.4. The antenna is a PE4099 SMA adapter protruding into the cavity to generate a very large ensemble of data, 1x1, 2x2, and 3x3 cavity scattering matrices $\overleftrightarrow{S}$.

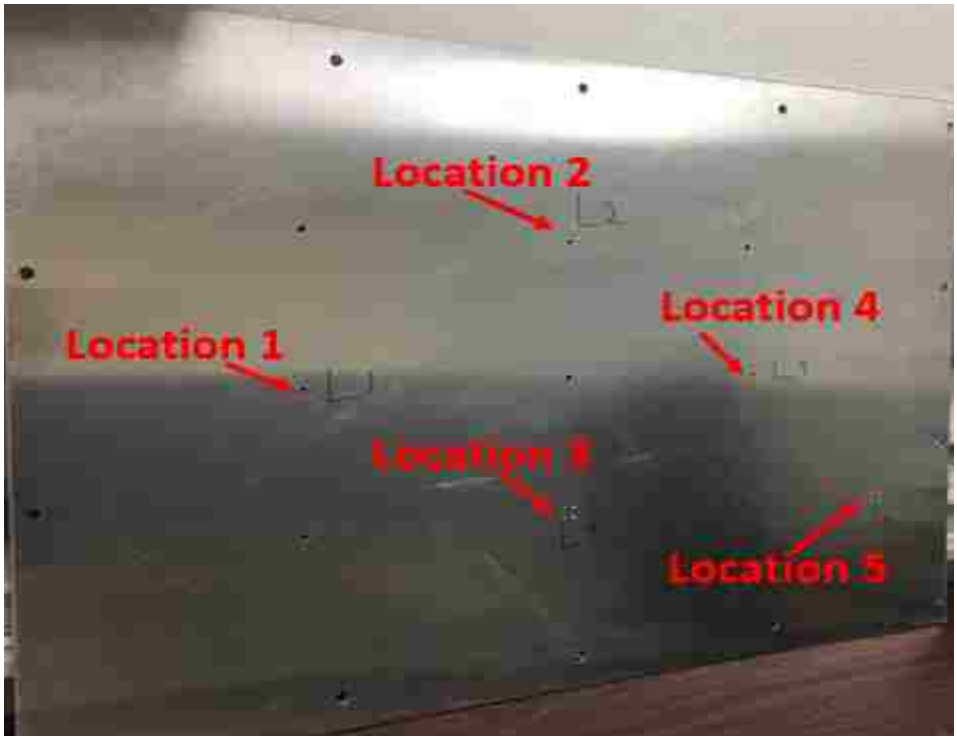

Fig. 2.3. Photograph of a surface of a quasi-3D cavity and antenna locations.

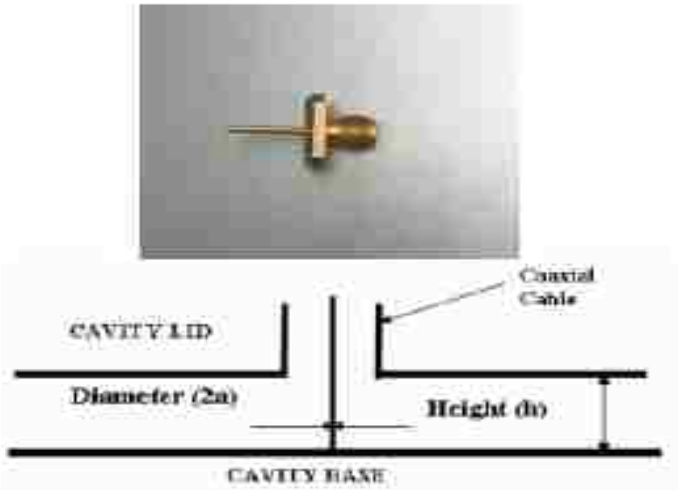

Fig. 2.4. Photograph of a PE4099 SMA adapter (top) used as an antenna (bottom).

In addition, we use 50 Ω transmission lines of different lengths to connect the cavity to the PNA-X.

2.3.1 Experimental Radiation Impedance Normalization Process in One-Port Systems

To validate that our quasi-2D cavities are in fact wave-chaotic we use Dyson's circular ensemble hypothesis to verify the statistical independence of the phase and magnitude of the normalized eigenvalues. We validated this hypothesis by decomposing the eigenvalues of the normalized super vector $\overleftrightarrow{s}$ and then grouping the complex eigenvalues into a set λ_s. We verify Dyson's circular ensemble hypothesis when the quasi-2D cavity is excited through one port, two ports, and three ports.

Using a cavity with no inserts and an antenna protruding into the cavity through one port at antenna location 2 specified in Fig. 2.3, and using the vector network analyzer (VNA) we connect one port to the cavity and we extract $\overleftrightarrow{S}$ as a function of frequency. We then convert the

super-matrix 100001×200 of $\overleftrightarrow{S}$ into $\overleftrightarrow{s}$ to calculate λ_s using the equations in Section 2.1 to verify the existence of chaotic rays through Dyson's circular ensemble hypothesis. Fig. 2.5 is an example of Dyson's hypothesis for a frequency range of 10.0-10.5 GHz. Using our experimentally-generated data, we calculate the loss parameter to be α=0.7562.

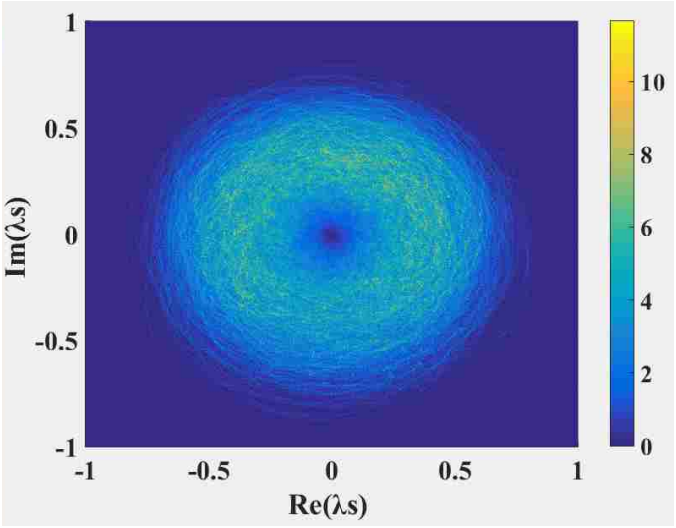

Fig. 2.5. Polar contour density plot of the real part of λ_s vs. the imaginary part of λ_s for a one-port measurement.

Using the experimentally determined value of α in a MC simulation of the RMT we generate a large statistical matrix of normalized impedances ($\overleftrightarrow{z}$), which can then be compared with the experimental and theoretical RCM-generated PDFs for the real and imaginary of the eigenvalues of the normalized impedance; we see an excellent agreement, as shown in Fig. 2.6 and Fig. 2.7.

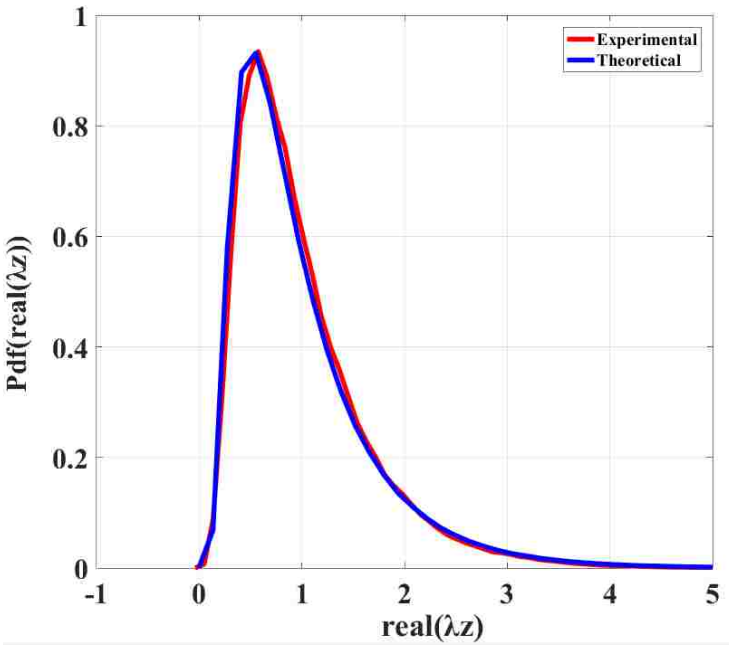

Fig. 2.6. Comparison of experimental measurements (red) and theoretical simulations (blue) of the PDFs of the real part of the eigenvalues of the normalized impedance for a one-port measurement.

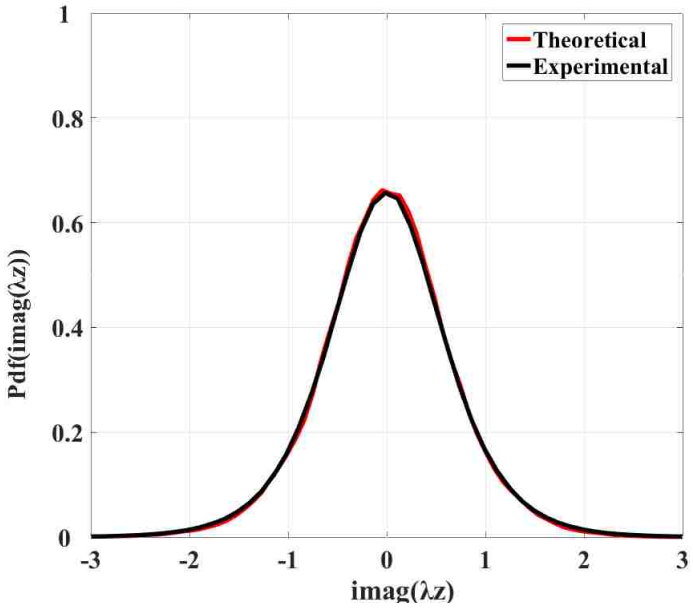

Fig. 2.7. Comparison of experimental measurements (black) and theoretical simulations (red) of the PDFs of the imaginary part of the eigenvalues of the normalized impedance.

2.3.2 Experimental Radiation Impedance Normalization Process in Two-Port Systems

A quasi-2D cavity with a bowtie insert and with two antennas protruding into the cavity through port one at antenna location 5 and port two through antenna location 3 (antenna locations specified in Fig. 2.3) was tested. Using the VNA we connect two ports to the cavity and we extract $\overleftrightarrow{S}$ as a function of frequency. We convert the super-matrix $2\times2\times100001\times200$ of $\overleftrightarrow{S}$ into $\overleftrightarrow{s}$ to calculate λ_s using the equations in Section 2.1 We verify the existence of wave-chaotic rays through Dyson's circular ensemble hypothesis, as shown in Fig. 2.8. Fig. 2.8 is an example of Dyson's hypothesis for the frequency range of 10.0-10.2 GHz. Using our experimentally-generated data, we calculate the loss parameter for this case to be α=1.4052. Given this value of α the MC simulation of the RMT generates a large statistical 2×2 matrix of normalized impedances ($\overleftrightarrow{z}$). We compare the experimental and theoretical RCM-generated PDFs for the real and imaginary parts of the eigenvalues of the normalized impedance (Fig. 2.9 and Fig. 2.10).

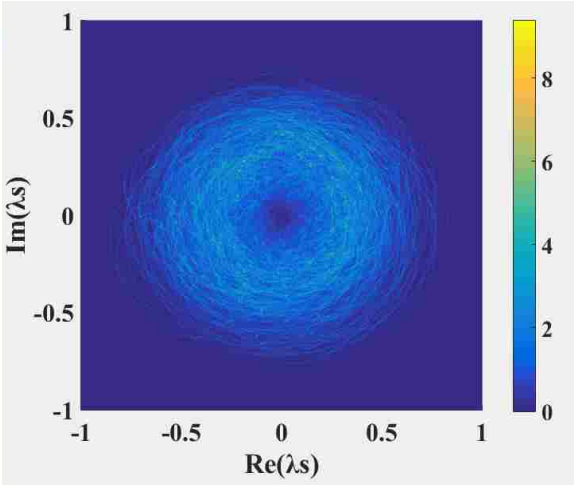

Fig. 2.8. Polar contour density plot of the real part of λ_s vs. the imaginary part of λ_s for a two-port measurement.

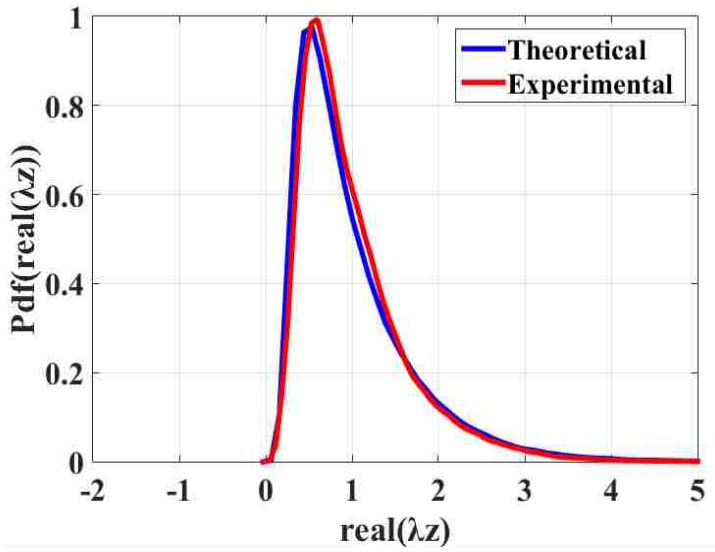

Fig. 2.9. Comparison of the experimental measurements (red) and theoretical simulations (blue) of the PDFs of the real part of the eigenvalues of the normalized impedance for a two-port measurement.

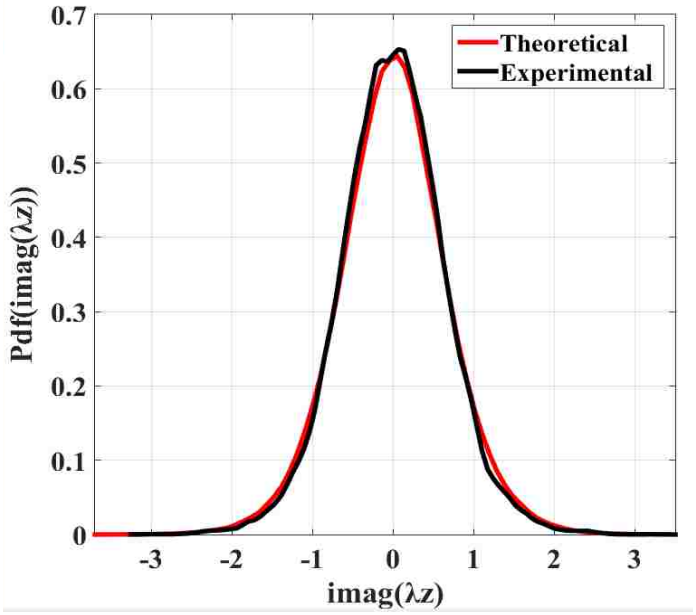

Fig. 2.10. Comparison of the experimental measurements (black) and theoretical simulations (red) of the PDFs of the imaginary part of the eigenvalues of the normalized impedance for a two-port measurement.

2.3.3 Experimental Radiation Impedance Normalization Process for Three-Port Systems

Measurements were performed using a cavity with an elliptical insert and using 3 antennas protruding into the cavity through port one at antenna location 1, port two at antenna location 4, and port three at location 5 (antenna locations specified in Fig. 2.3). Using the VNA we connect two ports to the cavity and we extract $\overleftrightarrow{S}$ as a function of frequency. We convert the $3\times3\times100001\times200$ $\overleftrightarrow{S}$ into $\overleftrightarrow{s}$ to calculate λ_s using the equations in Section 2.1 to verify the existence of chaotic waves through Dyson's circular ensemble hypothesis. Fig. 2.11 is an example of Dyson's hypothesis for the frequency range 10.1-10.2 GHz. Using our experimentally-generated data, we calculate the loss parameter for this case to be α=1.7471. Given this value of α the MC simulation of the RMT generates a large statistical 3×3 matrix of normalized impedance ($\overleftrightarrow{z}$). We compare the experimental and theoretical RCM-generated PDFs for the real and imaginary of the eigenvalues of the normalized impedance in Figs 2.12 and Fig. 2.13.

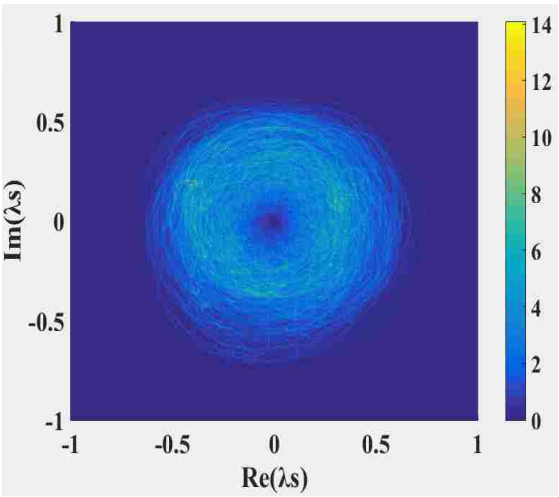

Fig. 2.11. Polar contour density plot of the real part of λ_s vs. the imaginary part of λ_s for a three-port measurement.

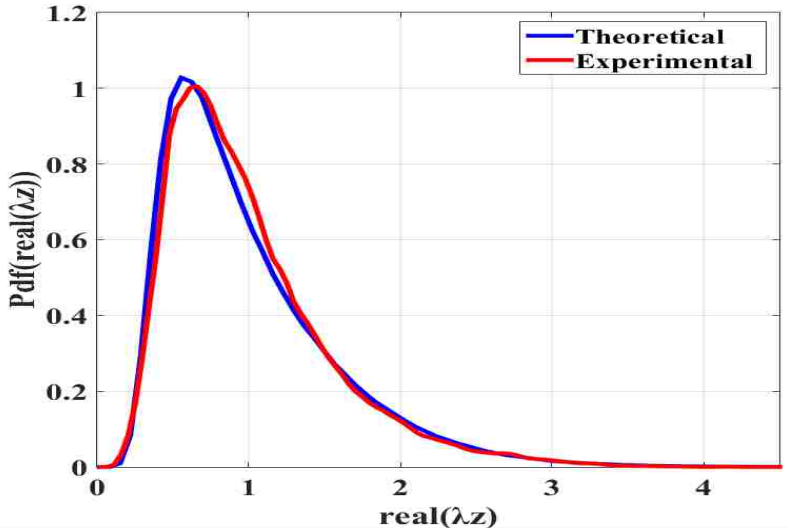

Fig. 2.12. Comparison of the experimental measurements (red) and theoretical simulations (blue) of the PDFs of the real part of the eigenvalues of the normalized impedances for a three-port measurement.

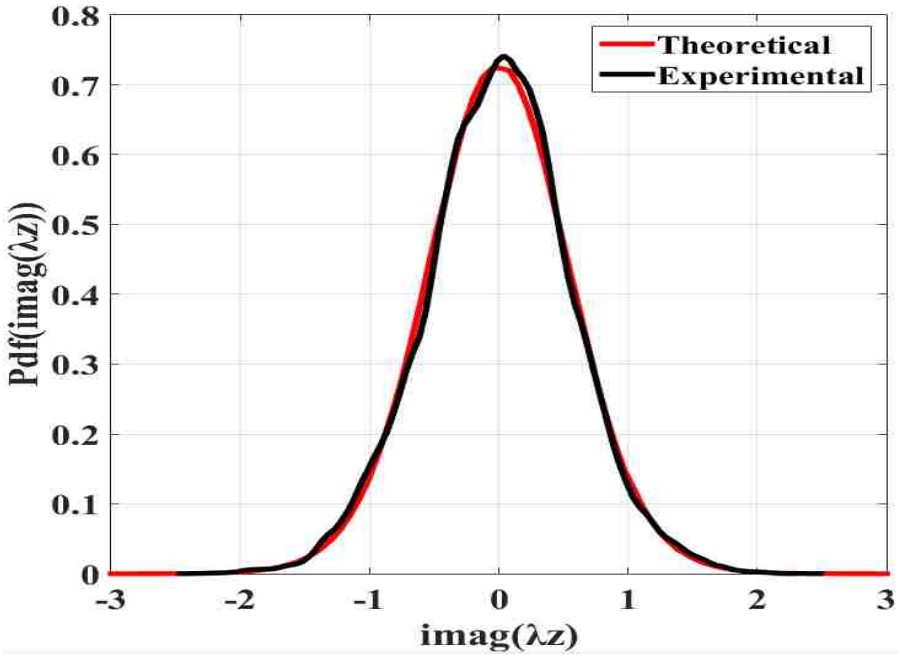

Fig. 2.13. Comparison of the experimental measurements (black) and theoretical simulations (red) of the PDFs of the imaginary part of the eigenvalues of the normalized impedance for a three-port measurement.

We observed for all cavities with different inserts that they become wave-chaotic cavities when excited by one port, two ports, and three ports at frequencies of 3.5 GHz and higher, and the loss parameter increases as a function of frequency. Fig. 2.14 presents the cavity loss factor as a function of frequency for a cavity with a bi-elliptical insert. We observe that the loss parameter increases as a function of frequency; the magenta lines refer to the loss parameter calculated using Eq. (2.11) leading to Re[$\overleftrightarrow{z}$], and the blue blocks give Im[$\overleftrightarrow{z}$]; the cases where only one color is shown is where both blocks overlap each other.

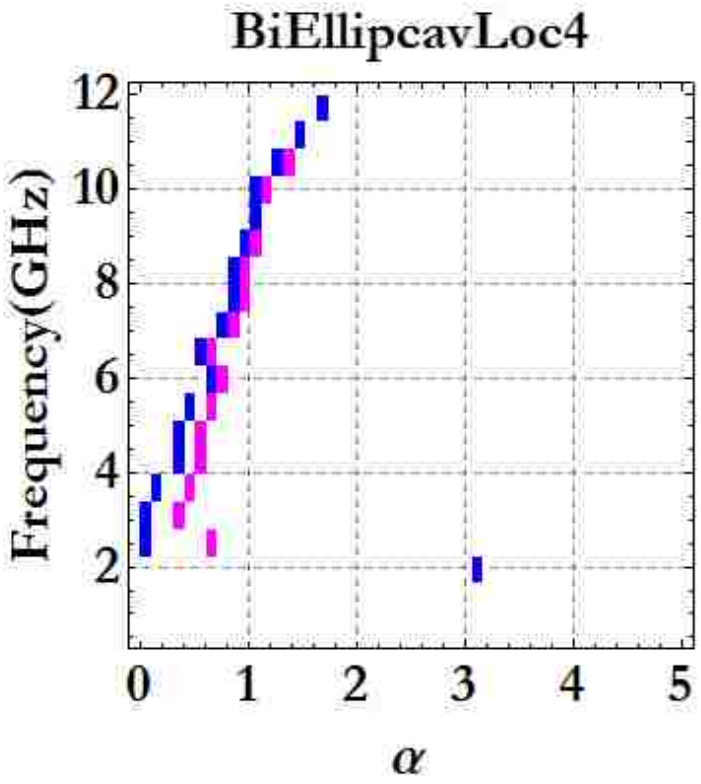

Fig. 2.14. Experimental measurements of loss parameter as a function of frequency in a quasi-2D cavity with a bi-elliptical insert.

In these experiments, once we obtain the normalized scattering coefficient $\overleftrightarrow{s}$ we can experimentally validate the statistical predictions for the magnitude and the phase of $\overleftrightarrow{s}(\varphi_s)$ using

the RCM. We can see that at higher frequencies the PDF of φ_s approaches a uniform distribution and at lower frequencies, the PDF of φ_s is not uniformly distributed. Fig. 2.15 is one example of many verifications we performed for one-port measurements.

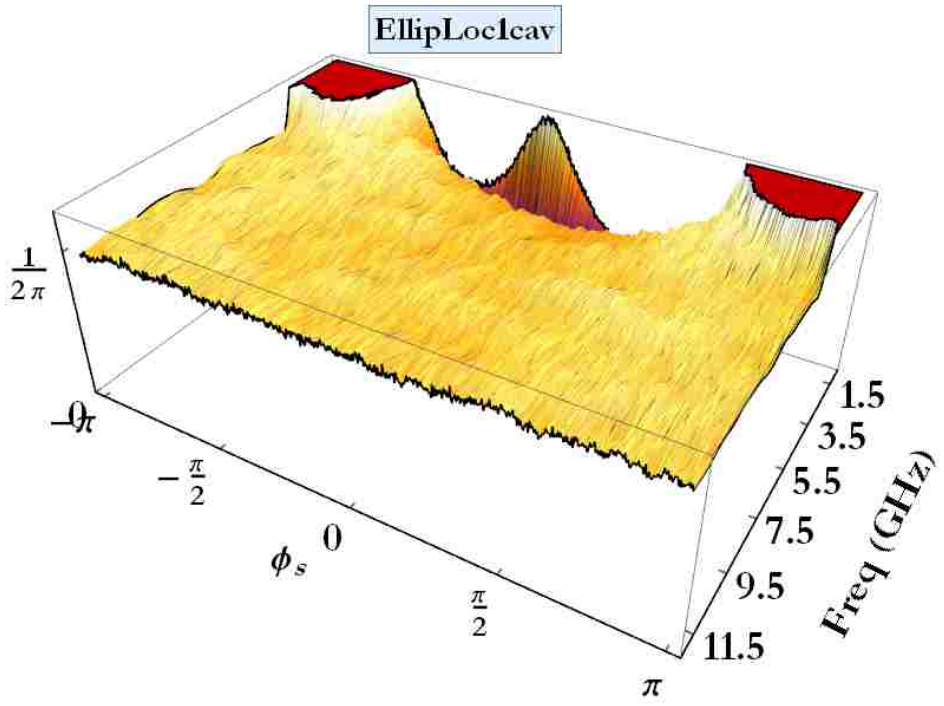

Fig. 2.15. The PDF of the phase angle φ_s of the normalized scattering coefficient $\vec{s}$.

We calculate the mean square error (MSE) Ω for the sum of all the $P(\varphi_s)$ of all the one-port measurements where φ_s is the phase angle of the normalized scattering parameter ($\vec{s}$) (Fig. 2.16) using

$$\Omega = \sum \left(P(\varphi s) - \frac{1}{2\pi} \right)^2. \tag{2.14}$$

We found that the MSE for the frequency range 6-12 GHz becomes very small and, therefore, we decided to continue our study of wave-chaotic waves within this range.

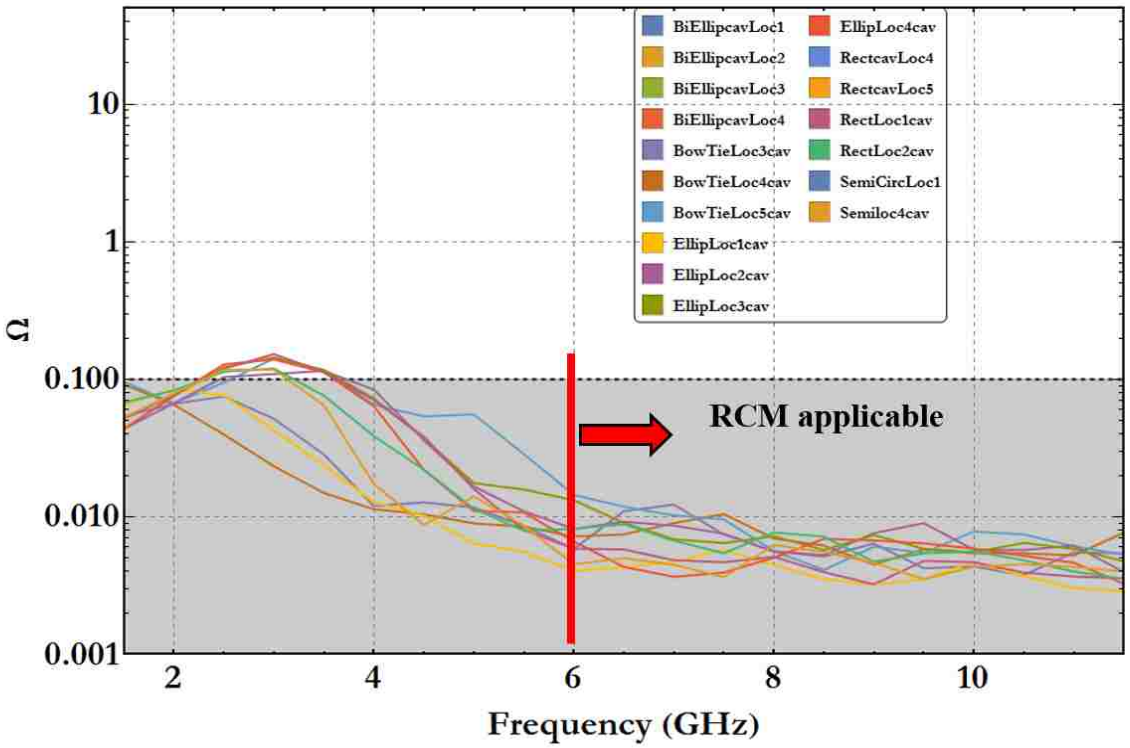

Fig. 2.16. PDF MSE distance as a function of frequency for one-port testing.

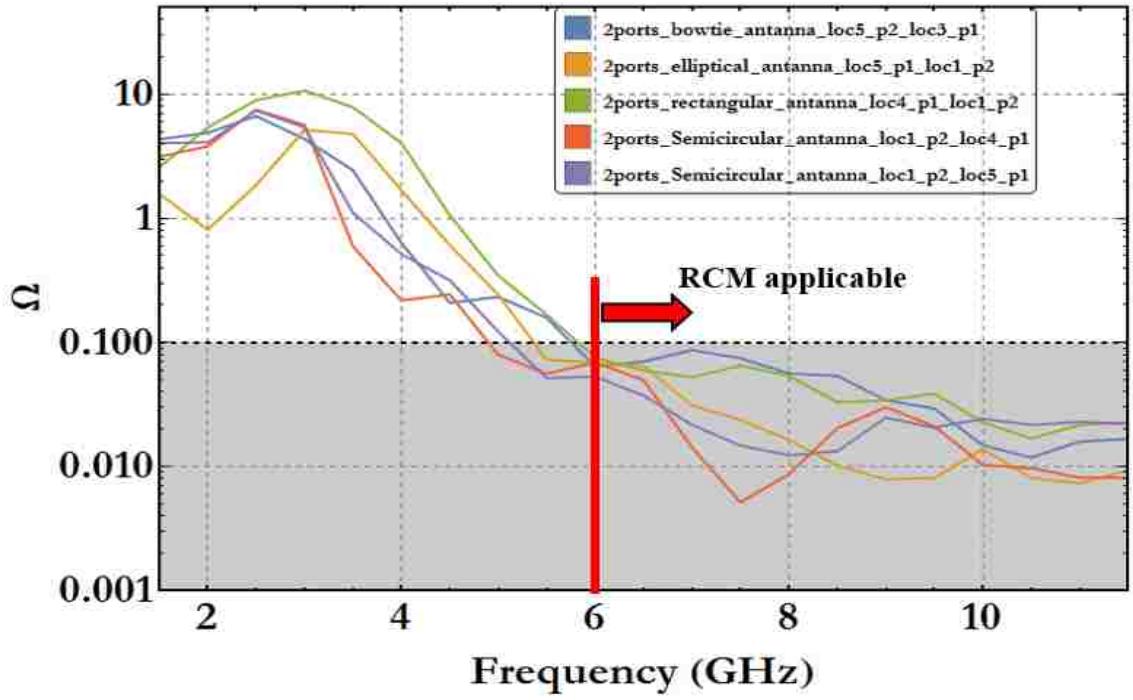

Fig. 2.17. PDF MSE distance as a function of frequency for two-port testing.

As a conclusion to this section, all of our quasi-2D cavities are ray-chaotic enclosures and the RCM is applicable, and we can further use them to create a network of cavities to mimic a real-world facility.

2.4 The Radiation Case

The radiation case involves obtaining coefficients of $\overleftrightarrow{S}$ for the excitation port when waves enter the cavity and do not return to the port. This condition is achieved by distributing commercial microwave absorbers (ECCOSORB® LS-24 and ECCOSORB MCS) along the side walls of the cavity, which provides about 40 dB of reflection loss when the frequency is between 6 and 12 GHz. For this experiment, we use our quasi-2D cavity with semicircular inserts. The first case we test for is where there are no absorbers along the boundaries (we call this loss case 0); the second case is loss case 1 (where 2 cm long sections of absorber are distributed evenly along the perimeter of the cavity and spaced 10 cm apart, as shown in Fig. 2.18); the third case is loss case 2 (where 2 cm long sections of absorber are evenly distributed along the perimeter of the cavity and spaced 5 cm apart, as shown in Fig. 2.19); and the final case is loss case 3 (where absorbers are distributed all along the perimeter, as shown in Fig. 2.20). In all cases, we excited the cavities using two ports, port 1 at location 5 and port 2 at location 3.

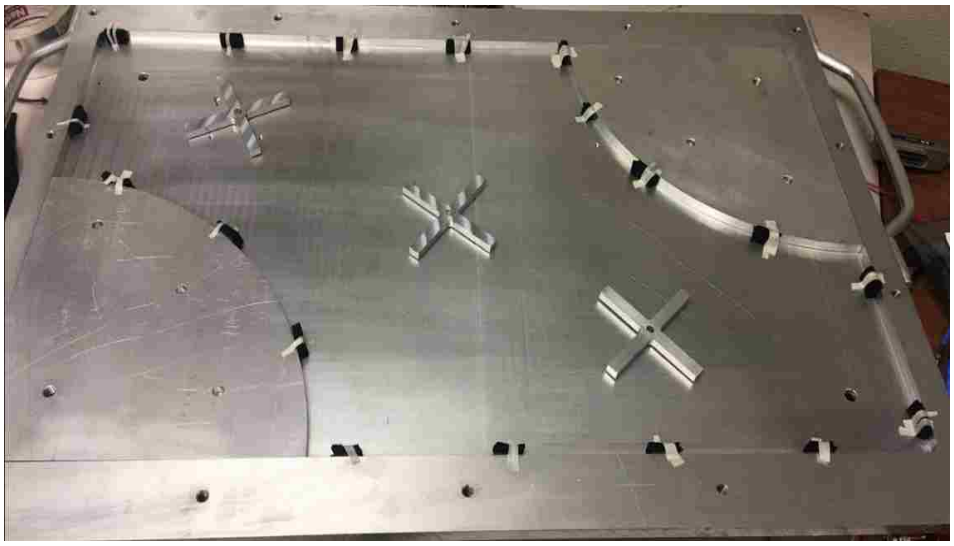

Fig. 2.18. Photograph of the quasi-2D cavity for loss case 1.

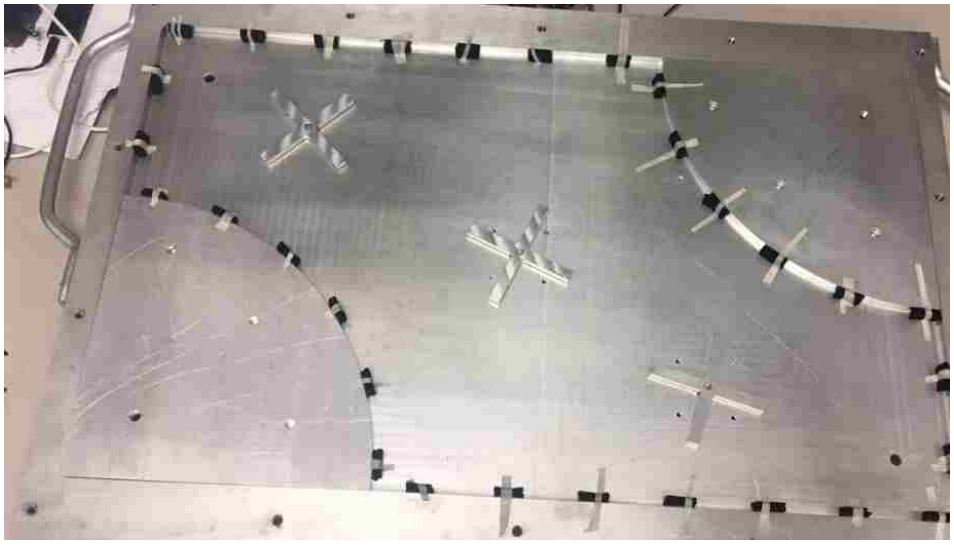

Fig. 2.19. Photograph of the quasi-2D cavity for loss case 2.

Fig. 2.20. Photograph of the quasi-2D cavity for loss case 3.

As we increase the amount of absorber material placed inside the cavity, the loss parameter increases and the cavities are still chaotic, as shown in Fig. 2.21 and Fig. 2.22.

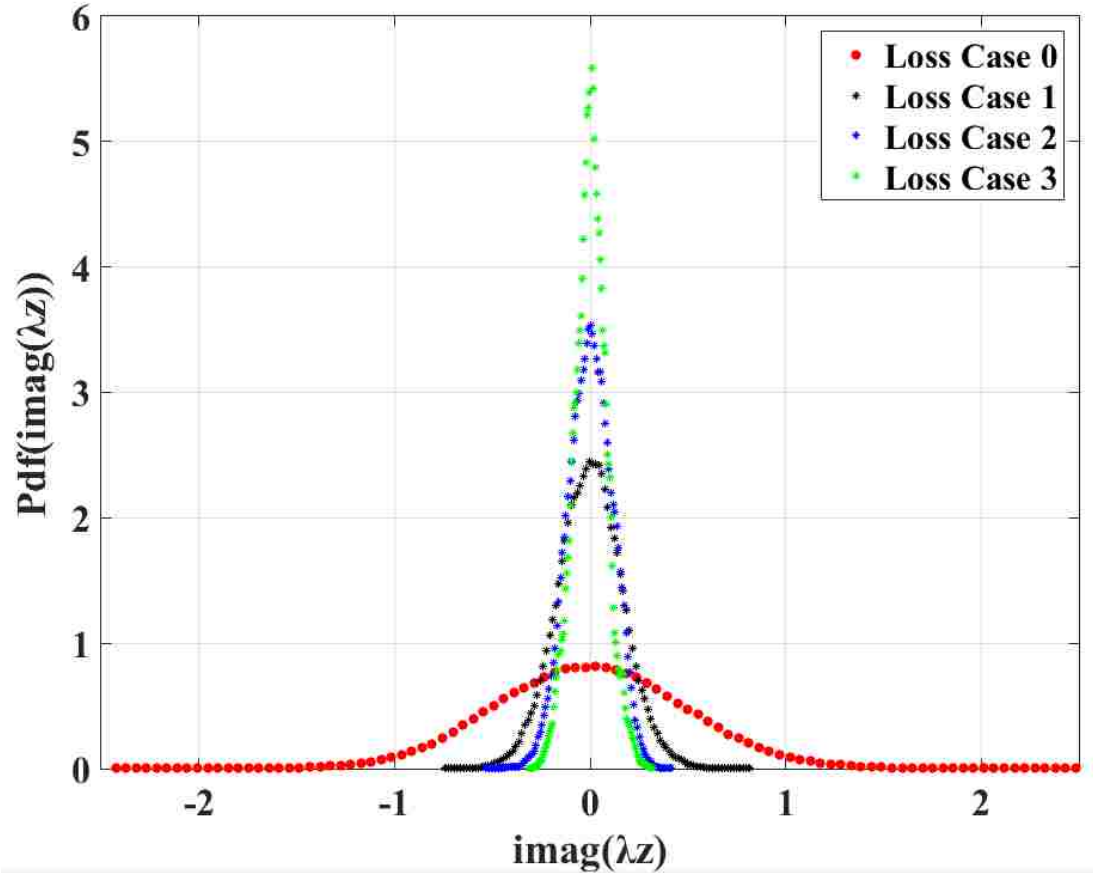

Fig. 2.21. Experimentally obtained PDFs of the imaginary part of the eigenvalues of the normalized impedances for all the radiation loss cases.

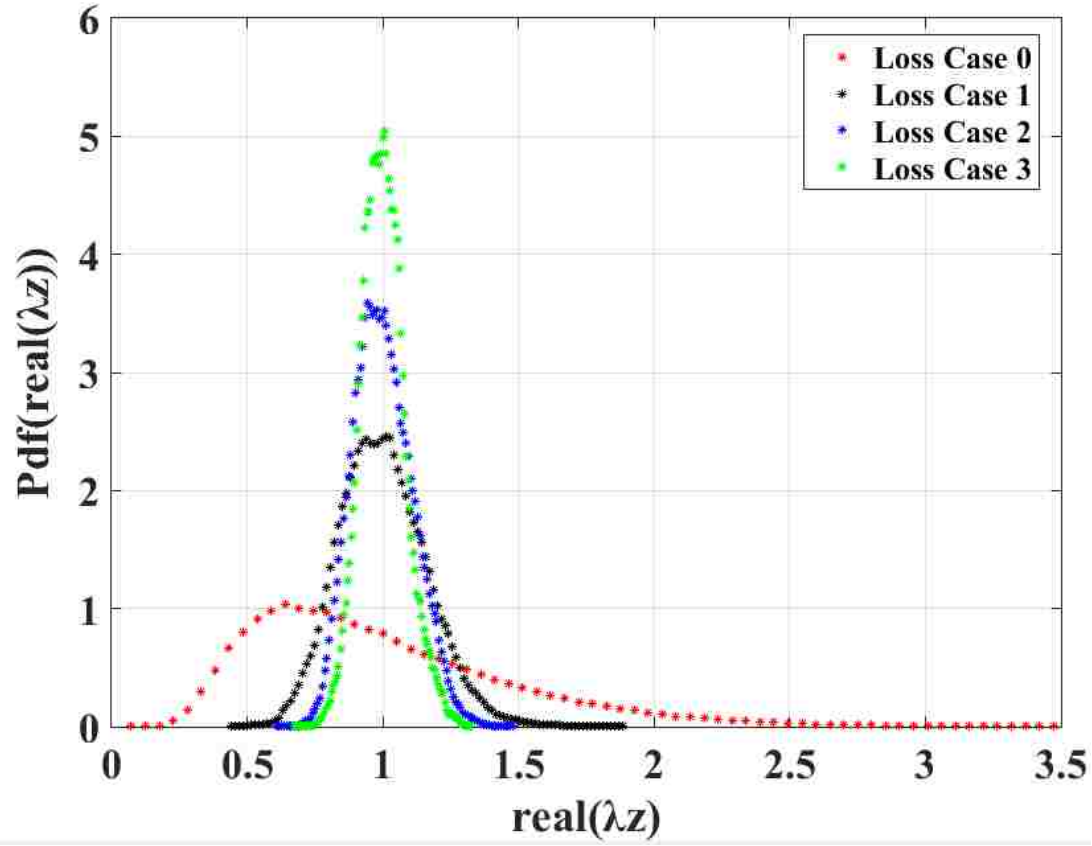

Fig. 2.22. Experimentally obtained PDFs of the real part of the eigenvalues of the normalized impedances for all the radiation loss cases.

We also measure the results of the radiation scattering coefficient S_{rad} over the same frequency range 6-12 GHz to show the fluctuations introduced into the measurement of S_{rad} due to the waves that leave the port and bounce on cavity walls and return to the port. The more we increase the absorbers around the walls the fewer are the waves that return. The magnitude of S_{rad} is shown in Fig. 2. 23.

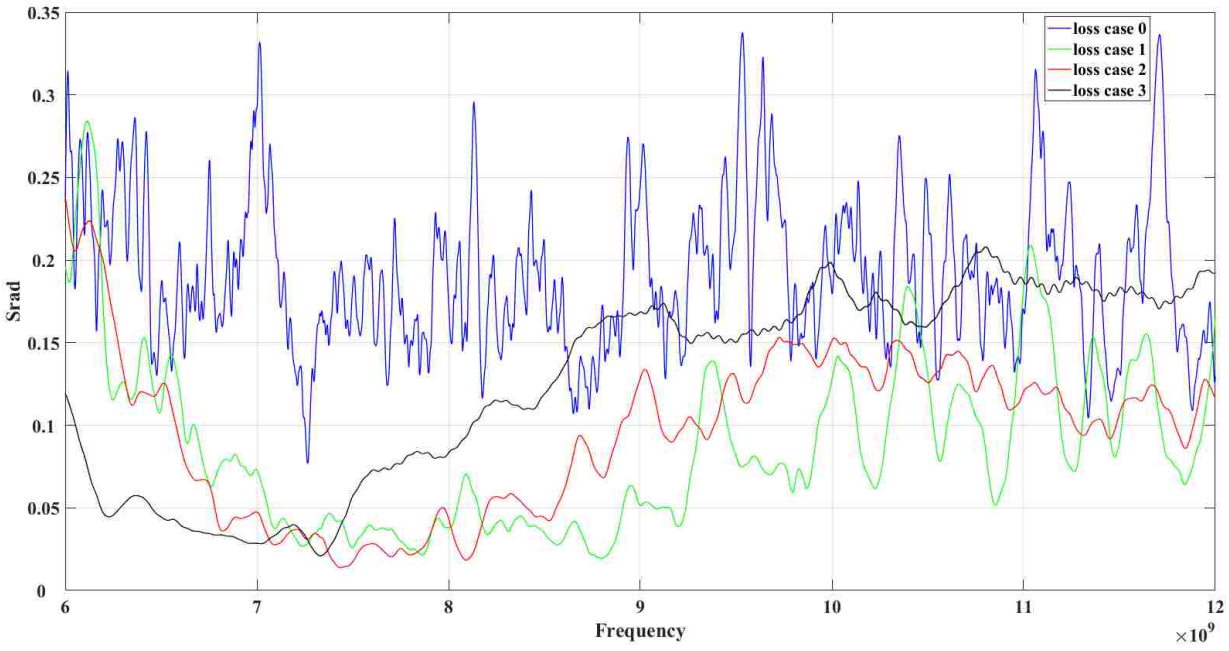

Fig. 2.23. Magnitude of the measured values of S_{rad}.

Chapter 3: The Baum-Liu-Tesche (BLT) Electromagnetic Topology Model

The BLT electromagnetic topology model involves the division of a complex electromagnetic problem into smaller problems that are easier to solve [6]. The BLT electromagnetic topology model makes excellent use of the "good shielding approximation" principle, which assumes that the inner volumes do not interact with the external volumes. Sub-volumes are volumes consisting of walls and cables. There are two types of walls: walls with proper shielding that provide physical separation between the volumes and walls with not so good shield (e.g. have some apertures or wires connected to other walls, will leak energy to other volumes). "A BLT network can be seen as a formulation of the electromagnetic coupling existing between the different volumes, which compose the entire volume under study" [7]. The BLT electromagnetic topology model is a hierarchical framework based on the MTL model for describing the flow of energy between different nodes on a network of MTL segments.

The electromagnetic interaction within the BLT is represented by the BLT equation:

$$\{\overleftrightarrow{I} - \overleftrightarrow{S} \cdot \overleftrightarrow{\Gamma}\} \cdot [W(0)] = \overleftrightarrow{S} \cdot [W_S], \tag{3.1}$$

where $\overleftrightarrow{I}$, $\overleftrightarrow{S}$, and $\overleftrightarrow{\Gamma}$ are the identity, scattering, and propagation super-matrices, respectively. [W(0)] and $[W_S]$ represent the outgoing and the source waves, respectively. In a BLT network of volumes, volumes are described in terms of junctions. Junctions are related to each other through tubes, and tubes represent the forward and backward traveling waves through apertures or transmission lines. The BLT equation can then be used to calculate the voltage and the current responses at each junction in a network's sub-volume.

The advantage of using the electromagnetic topology in the frequency domain is that the different sub-volumes can be treated independently. The elements of the super-matrices are

determined either through numerical methods for computational electromagnetics, or through analytic expressions.

We represent the 2D aluminum cavities as volumes within the BLT network; the junctions are represented by the radiation impedances at each port, and the transmission lines are represented by the coaxial cables. We want to apply the BLT equation to a network of arbitrarily connected cavities by using $\overleftrightarrow{S}$ derived from the RCM for each cavity so we can directly compute the induced currents and voltages.

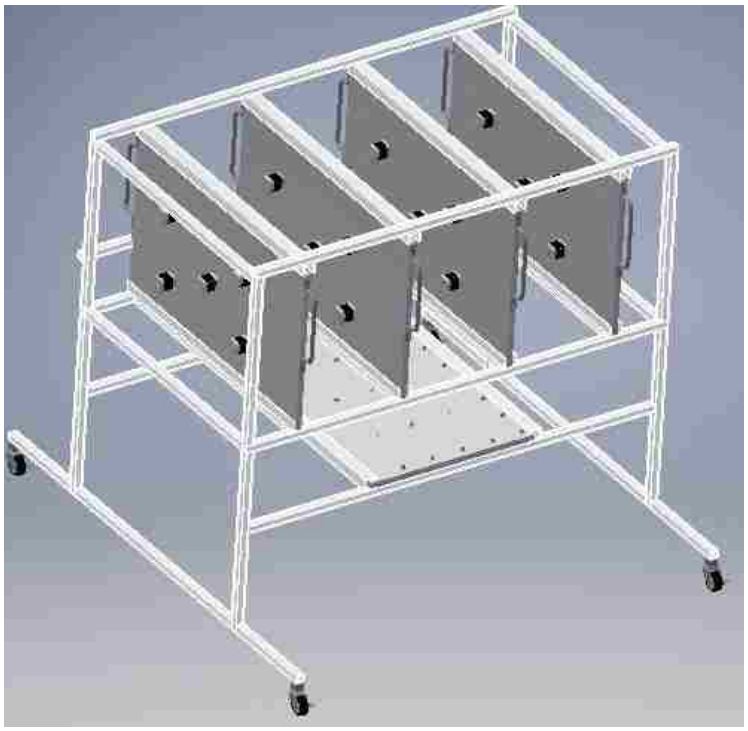

Fig. 3.1. CAD drawing of five quasi-2D ray chaotic cavities that will be interconnected in an arbitrary manner.

The cavities are either arbitrarily connected or in a cascaded fashion using 50 Ω coaxial transmission lines, as we will see later in this chapter. The electromagnetic interaction within the network is then represented by a topological network for the three randomly interconnected cavities. In this Dissertation, we express each volume in the BLT network via an experimentally-

generated $\overleftrightarrow{S}$, and a numerical simulation-generated $\overleftrightarrow{S}$ using MC MATLAB simulations for purposes of comparison.

3.1 Experimental BLT Formulation for Interconnected Cavities

The BLT formalism requires a geometric description of the problem in order to break it down to establish an interaction graph between the volumes and a description of the propagation through the interfaces. The first network configuration of BLT we performed was for three cavities arbitrarily connected. In this case we are working in the frequency range of 6-12 GHz.

Cavity A: A quasi-2D cavity with a bowtie-shaped insert that is excited by three ports at location 3, location 4, and location 5.

Cavity B: a quasi-2D cavity with an elliptically-shaped insert that is excited by three ports at location 1, location 4, and location 5.

Cavity C: a quasi-2D cavity with a semicircularly-shaped insert that is excited by two ports at location 1 and location 5.

We connected the cavities to each other and to the VNA, as shown as shown in Fig. 3.2. A photograph of the set-up is shown in Fig. 3.3.

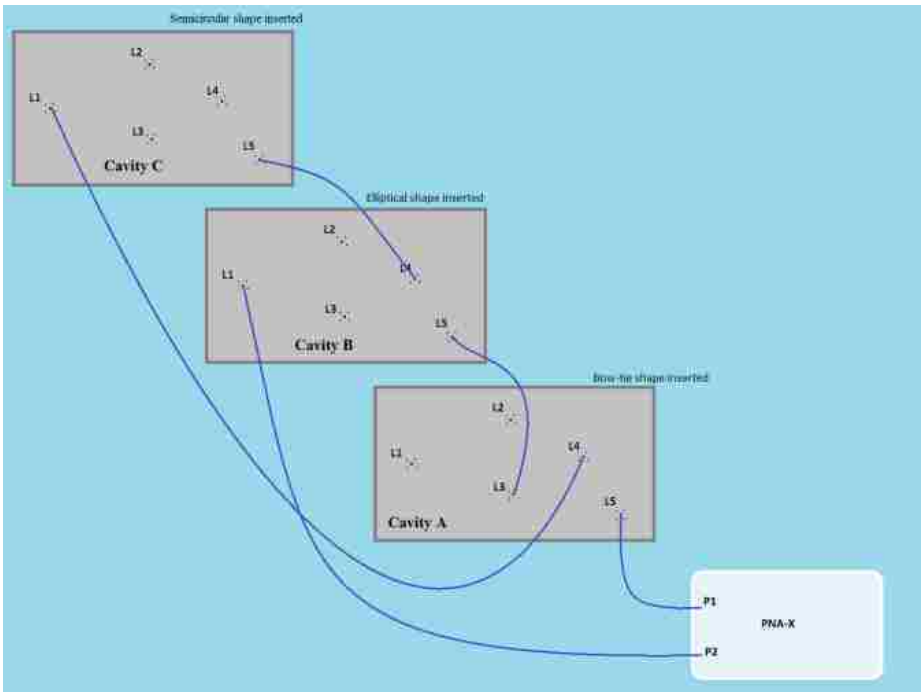

Fig. 3.2. Schematic of the experimental setup for three interconnected cavities forming the BLT network topology.

Fig. 3.3. Photograph of the experimental setup for three interconnected cavities.

Cavities A and B both have two mode stirrers, and cavity C has three mode stirrers. On all the cavities, we have multiple stepper motors rotating so that the mode stirrers move at the same time at each rotation. Using an Arduino shield on top of the Arduino UNO processor helped us in mounting several stepper motors on the cavity and rotating them simultaneously. All the mode stirrers rotate 200 times. At each rendition of the mode stirrer, we extract 100k complex scattering parameters $\overleftrightarrow{S}$ vs. frequency from the VNA.

We previously tested each cavity by themselves using the method presented in Chapter 2 for RCM applicability. We then generate $\overleftrightarrow{S}$ based on the number of ports exciting each cavity, and we calculate the loss parameter for each cavity. Cavity A is excited by three ports; therefore, Cavity A super-matrix $\overleftrightarrow{S}$ has size 3x3x100001x200, Cavity B super-matrix $\overleftrightarrow{S}$ has size 3x3100001x200, and Cavity C super-matrix $\overleftrightarrow{S}$ has size 3x3100001x200.

We represent the 2D aluminum cavities as volumes within the BLT network; the junctions are represented by the radiation impedances at each port, and the transmission lines are represented by the coaxial cables connecting the cavities to each other. We want to apply the BLT equation to a network of arbitrarily connected cavities by using $\overleftrightarrow{S}$ experimentally-generated for each cavity so that we can directly compute the induced currents and voltages. The corresponding BLT topological network for arbitrarily interconnected cavities is shown in Fig. 3.4. J0–J4 represent the excited voltage source, cavity A, cavity B, cavity C, and the matching resistance, respectively.

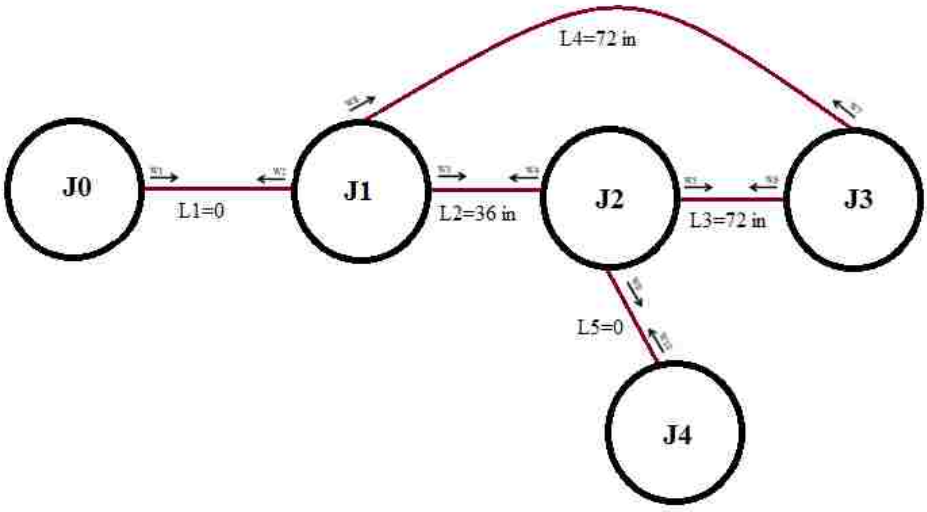

Fig. 3.4. BLT topological network for three randomly interconnected cavities.

Based on this topological MTL network we can build the electromagnetic interaction represented by the BLT equation. $W(1) - W(10)$ are the outgoing voltage waves and $W_S(1) - W_S(10)$ are the source waves. Thus, the relevant BLT equation is given by:

$$\{\overleftrightarrow{I} - \overleftrightarrow{S} \cdot \overleftrightarrow{\Gamma}\} \cdot \begin{bmatrix} W(1) \\ W(2) \\ W(3) \\ W(4) \\ W(5) \\ W(6) \\ W(7) \\ W(8) \\ W(9) \\ W(10) \end{bmatrix} = \overleftrightarrow{S} \cdot \begin{bmatrix} W_S(1) \\ W_S(2) \\ W_S(3) \\ W_S(4) \\ W_S(5) \\ W_S(6) \\ W_S(7) \\ W_S(8) \\ W_S(9) \\ W_S(10) \end{bmatrix}, \tag{3.2}$$

where $\overleftrightarrow{I}$ is the identity matrix (10 by 10) given by

$$\overleftrightarrow{I} = \begin{pmatrix} 1 & 0 & 0 & 0 & 0 & 0 & 0 & 0 & 0 & 0 \\ 0 & 1 & 0 & 0 & 0 & 0 & 0 & 0 & 0 & 0 \\ 0 & 0 & 1 & 0 & 0 & 0 & 0 & 0 & 0 & 0 \\ 0 & 0 & 0 & 1 & 0 & 0 & 0 & 0 & 0 & 0 \\ 0 & 0 & 0 & 0 & 1 & 0 & 0 & 0 & 0 & 0 \\ 0 & 0 & 0 & 0 & 0 & 1 & 0 & 0 & 0 & 0 \\ 0 & 0 & 0 & 0 & 0 & 0 & 1 & 0 & 0 & 0 \\ 0 & 0 & 0 & 0 & 0 & 0 & 0 & 1 & 0 & 0 \\ 0 & 0 & 0 & 0 & 0 & 0 & 0 & 0 & 1 & 0 \\ 0 & 0 & 0 & 0 & 0 & 0 & 0 & 0 & 0 & 1 \end{pmatrix}. \quad (3.3)$$

$\overleftrightarrow{S}$ corresponds to the measured or RCM-generated cavity scattering matrix. The $\overleftrightarrow{S}$ matrix is characterized by the incoming and outgoing wave at each junction. $\overleftrightarrow{S}$ is generated using a wave to wave matrix given by [8] two waves – W_i (incoming wave) and W_j (outgoing wave):

(W_i, W_j) = 1, if there is a junction J, W_i leaves J and W_j arrives on J

(W_i, W_j) = 0, otherwise.

For this BLT configuration, we will use the topological network shown in Fig. 3.4, with

$$(\mathrm{Wi}, \mathrm{Wj}) = \begin{pmatrix} 0 & 0 & 0 & 0 & 0 & 0 & 0 & 0 & 0 & 0 \\ 1 & 0 & 0 & 1 & 0 & 0 & 0 & 1 & 0 & 0 \\ 1 & 0 & 0 & 1 & 0 & 0 & 0 & 1 & 0 & 0 \\ 0 & 0 & 1 & 0 & 0 & 1 & 0 & 0 & 0 & 1 \\ 0 & 0 & 1 & 0 & 0 & 1 & 0 & 0 & 0 & 1 \\ 0 & 0 & 0 & 0 & 1 & 0 & 1 & 0 & 0 & 0 \\ 1 & 0 & 0 & 1 & 0 & 0 & 0 & 1 & 0 & 0 \\ 0 & 0 & 0 & 0 & 1 & 0 & 1 & 0 & 0 & 0 \\ 0 & 0 & 1 & 0 & 0 & 1 & 0 & 0 & 0 & 1 \\ 0 & 0 & 0 & 0 & 0 & 0 & 0 & 0 & 0 & 0 \end{pmatrix} \quad (3.4)$$

and $\overleftrightarrow{S}$ becomes

$$\overleftrightarrow{S} = \begin{pmatrix} 0 & 0 & 0 & 0 & 0 & 0 & 0 & 0 & 0 & 0 \\ S11a & 0 & 0 & S21a & 0 & 0 & 0 & S31a & 0 & 0 \\ S12a & 0 & 0 & S22a & 0 & 0 & 0 & S33a & 0 & 0 \\ 0 & 0 & S33b & 0 & 0 & S23b & 0 & 0 & 0 & S13b \\ 0 & 0 & S23b & 0 & 0 & S22b & 0 & 0 & 0 & S21b \\ 0 & 0 & 0 & 0 & S22c & 0 & S12c & 0 & 0 & 0 \\ S13a & 0 & 0 & S23a & 0 & 0 & 0 & S33a & 0 & 0 \\ 0 & 0 & 0 & 0 & S21c & 0 & S11c & 0 & 0 & 0 \\ 0 & 0 & S31b & 0 & 0 & S21b & 0 & 0 & 0 & S11b \\ 0 & 0 & 0 & 0 & 0 & 0 & 0 & 0 & 0 & 0 \end{pmatrix}. \quad (3.5)$$

When using MTLs, the propagation matrix $\overleftrightarrow{\Gamma}$ represents a piece of cable with uniform cross-section. The propagation matrix describes the wave propagation at each tube and the cable characteristics, where L is the length of the cable connecting the cavities. $\overleftrightarrow{\Gamma}$ is a diagonal symmetric matrix of W_i and W_j when there is propagation to be considered the block in the diagonal would be equal to the propagation characteristics and when there is no propagation the diagonal elements would be equal to 1.

$$\overleftrightarrow{\Gamma} = \begin{pmatrix} 1 & 0 & 0 & 0 & 0 & 0 & 0 & 0 & 0 & 0 \\ 0 & 1 & 0 & 0 & 0 & 0 & 0 & 0 & 0 & 0 \\ 0 & 0 & e^{-j\frac{2\pi f}{c}*L1} & 0 & 0 & 0 & 0 & 0 & 0 & 0 \\ 0 & 0 & 0 & e^{-j\frac{2\pi f}{c}*L1} & 0 & 0 & 0 & 0 & 0 & 0 \\ 0 & 0 & 0 & 0 & e^{-j\frac{2\pi f}{c}*L2} & 0 & 0 & 0 & 0 & 0 \\ 0 & 0 & 0 & 0 & 0 & e^{-j\frac{2\pi f}{c}*L2} & 0 & 0 & 0 & 0 \\ 0 & 0 & 0 & 0 & 0 & 0 & e^{-j\frac{2\pi f}{c}*L3} & 0 & 0 & 0 \\ 0 & 0 & 0 & 0 & 0 & 0 & 0 & e^{-j\frac{2\pi f}{c}*L3} & 0 & 0 \\ 0 & 0 & 0 & 0 & 0 & 0 & 0 & 0 & 1 & 0 \\ 0 & 0 & 0 & 0 & 0 & 0 & 0 & 0 & 0 & 1 \end{pmatrix}. \quad (3.6)$$

We insert $\overleftrightarrow{S}$ into the BLT equation generated by the RCM and calculate W5, which is S_{21} generated by the equation. Also, we insert $\overleftrightarrow{S}$ generated experimentally into the BLT equation and

calculate W5. Lastly, we measure S_{21} using two-port measurements established on the entire BLT network configuration (see Fig. 3.4) and the results we obtained for the PDFs of S_{21} in all cases were identical. In a nutshell, we perform three tests to validate our results:

- $\overleftrightarrow{S}$ is generated numerically using RMT, then used in the BLT formalism
- $\overleftrightarrow{S}$ is generated experimentally then used in the BLT formalism
- The BLT formalism is established experimentally for the cavities and $\overleftrightarrow{S}$ is measured.

We have previously validated that the RCM applies to the cavities above 6 GHz in Chapter 2 for one-port, two-port, and three-port measurements. Our results show an excellent agreement between experimentally and theoretically fusing the RCM with BLT. Fig. 3.5 results suggest that the fusing of the RCM with the BLT electromagnetic topology model accurately reproduces the PDF for the measured S_{21} obtained in the experiment.

Another network configuration we studied was two interconnected cavities.

Cavity A: a quasi-2D cavity with a bowtie-shaped insert excited by two ports at location 3 and location 5.

Cavity B: a quasi-2D cavity with an elliptically-shaped insert excited by two ports at location 1and location 5.

We connected the cavities to each other and to the VNA. We want to apply the BLT equation to the network of connected cavities by using $\overleftrightarrow{S}$ experimentally-generated for the corresponding topological BLT network shown in Fig. 3.6. J0–J3 represent the excited voltage source, cavity A and cavity B, the matching resistance.

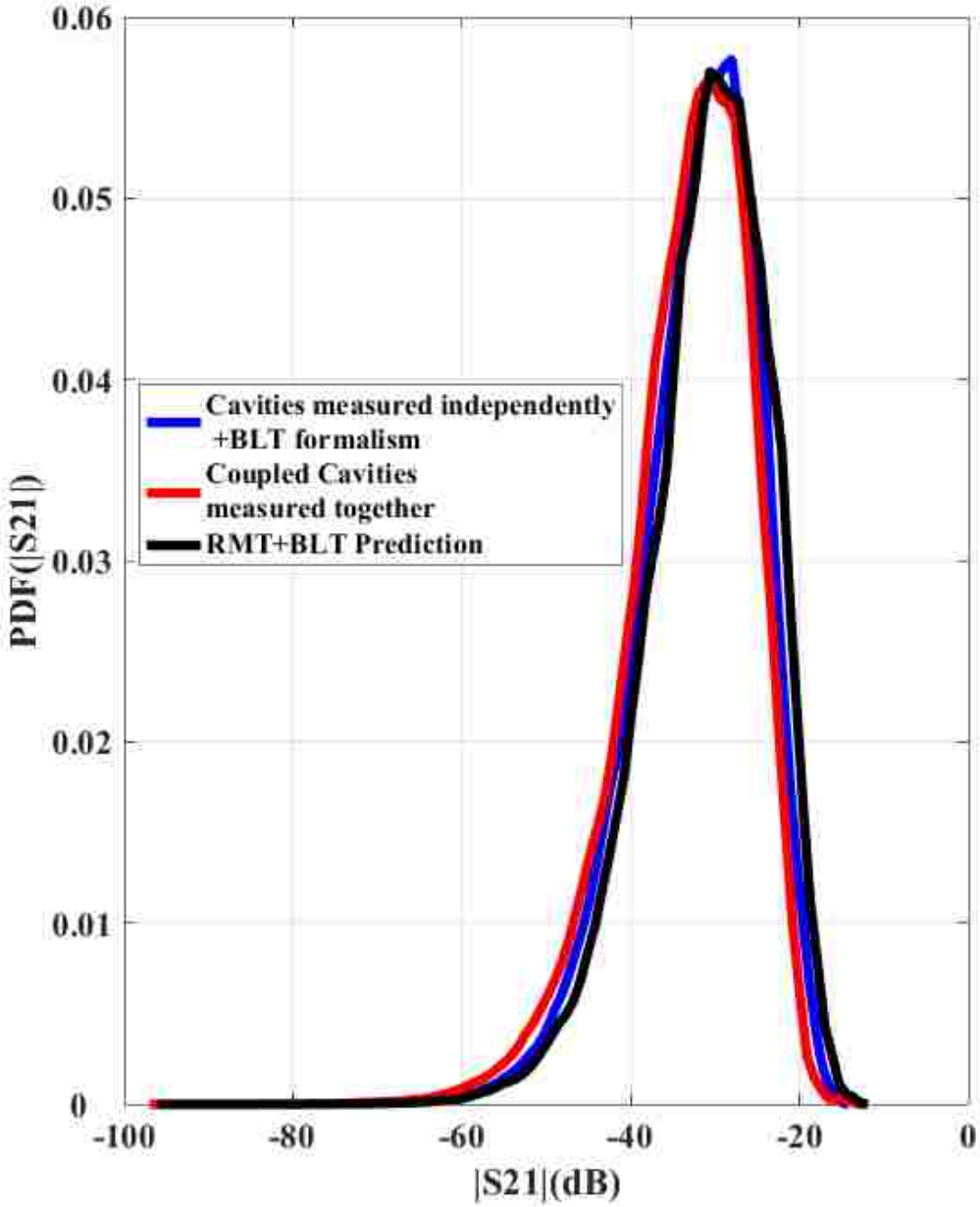

Fig. 3.5. BLT formalism results for three randomly interconnected cavities.

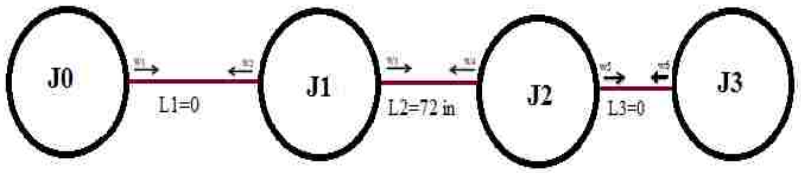

Fig. 3.6. BLT topological network for two interconnected cavities.

Based on this topological MTL network we can build the electromagnetic interaction represented by the BLT equation. $W(1) - W(6)$ are the outgoing voltage waves, $W_S(1) - W_S(6)$ are the source waves. Thus, the relevant BLT equation is given by:

$$\left\{\vec{\vec{\mathrm{I}}} - \vec{\vec{\mathrm{S}}} \cdot \vec{\vec{\Gamma}}\right\} \cdot \begin{bmatrix} \mathrm{W}(1) \\ \mathrm{W}(2) \\ \mathrm{W}(3) \\ \mathrm{W}(4) \\ \mathrm{W}(5) \\ \mathrm{W}(6) \end{bmatrix} = \vec{\vec{\mathrm{S}}} \cdot \begin{bmatrix} \mathrm{W_S}(1) \\ \mathrm{W_S}(2) \\ \mathrm{W_S}(3) \\ \mathrm{W_S}(4) \\ \mathrm{W_S}(5) \\ \mathrm{W_S}(6) \end{bmatrix}, \tag{3.7}$$

where $\vec{\vec{I}}$ is the identity matrix (6 by 6) given by

$$\vec{\vec{I}} = \begin{pmatrix} 1 & 0 & 0 & 0 & 0 & 0 & 0 & 0 \\ 0 & 1 & 0 & 0 & 0 & 0 & 0 & 0 \\ 0 & 0 & 1 & 0 & 0 & 0 & 0 & 0 \\ 0 & 0 & 0 & 1 & 0 & 0 & 0 & 0 \\ 0 & 0 & 0 & 0 & 1 & 0 & 0 & 0 \\ 0 & 0 & 0 & 0 & 0 & 1 & 0 & 0 \\ 0 & 0 & 0 & 0 & 0 & 0 & 1 & 0 \\ 0 & 0 & 0 & 0 & 0 & 0 & 0 & 1 \end{pmatrix}, \tag{3.8}$$

and $\vec{\vec{S}}$ corresponds to the measured or RCM-generated cavity scattering matrix. The $\vec{\vec{S}}$ matrix is characterized by the incoming and outgoing wave at each junction

$$\vec{\vec{S}} = \begin{pmatrix} 0 & 0 & 0 & 0 & 0 & 0 & 0 \\ S11a & 0 & 0 & S21a & 0 & 0 & 0 \\ S12a & 0 & 0 & S22a & 0 & 0 & 0 \\ 0 & 0 & S11b & 0 & 0 & S21b & 0 \\ 0 & 0 & S12b & 0 & 0 & S22b & 0 \\ 0 & 0 & 0 & 0 & 0 & 0 & 0 \end{pmatrix}. \tag{3.9}$$

The propagation matrix $\vec{\vec{\Gamma}}$ describes wave propagation at each tube and the cable characteristics, and L is the length of the cable connecting the cavities

$$\overleftrightarrow{\Gamma} = \begin{pmatrix} 1 & 0 & 0 & 0 & 0 & 0 \\ 0 & 1 & 0 & 0 & 0 & 0 \\ 0 & 0 & e^{-j\frac{2\pi f}{c}*L1} & 0 & 0 & 0 \\ 0 & 0 & 0 & e^{-j\frac{2\pi f}{c}*L1} & 0 & 0 \\ 0 & 0 & 0 & 0 & 1 & 0 \\ 0 & 0 & 0 & 0 & 0 & 1 \end{pmatrix}. \quad (3.10)$$

In these equations, we use $\overleftrightarrow{S}$ generated by the RCM and the expected PDFs should be identical to when we use the experimentally-generated $\overleftrightarrow{S}$, and the results should be identical to the PDFs of the measured $\overleftrightarrow{S}$ of the entire interconnected multiple cavity network. (We also measured S parameters while all the cavities are connected.)

We have validated that the RCM applies to the cavities above 6 GHz in Chapter 2 for 1-port, 2-port, and 3-port measurements. Our results (Fig. 3.7) show good agreement between experimentally and theoretically fusing the RCM with the BLT electromagnetic topology model for two interconnected cavities.

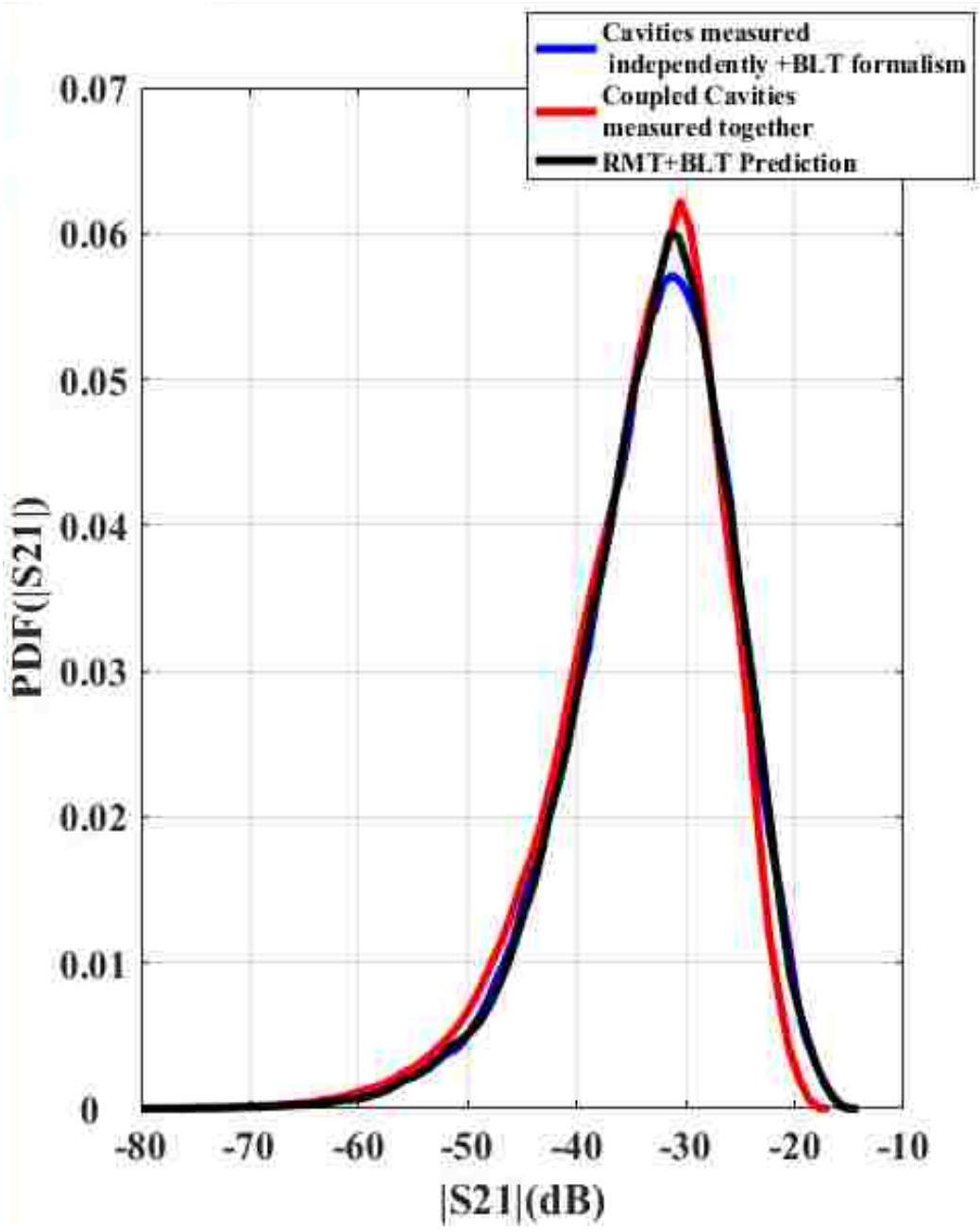

Fig. 3.7. BLT formalism results for two interconnected cavities.

3.2 Cascaded BLT Configurations

To further verify the BLT analysis, we studied different network configurations of the 2D cavities. One of the configurations is a network of cascaded cavities using the schematic in Fig. 3.8. The first cavity is excited by a source and power leaking out excites the subsequent cavities.

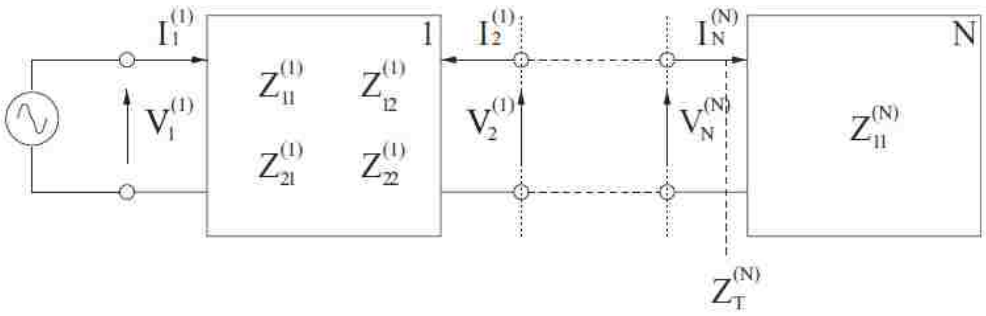

Fig. 3.8. Network model of a chain of coupled cavities.

The cavities are identical and with bowtie inserts, and all cavities are excited at the same antenna locations. The following graphs are results for two cascaded cavities with port 1 connected to the antenna at location 3. Using a transmission line of 62" we connected the antenna at location 5 of the first cavity to the antenna at location 3 of the second cavity, and the second cavity is connected to the PNA-X through antenna location 5.

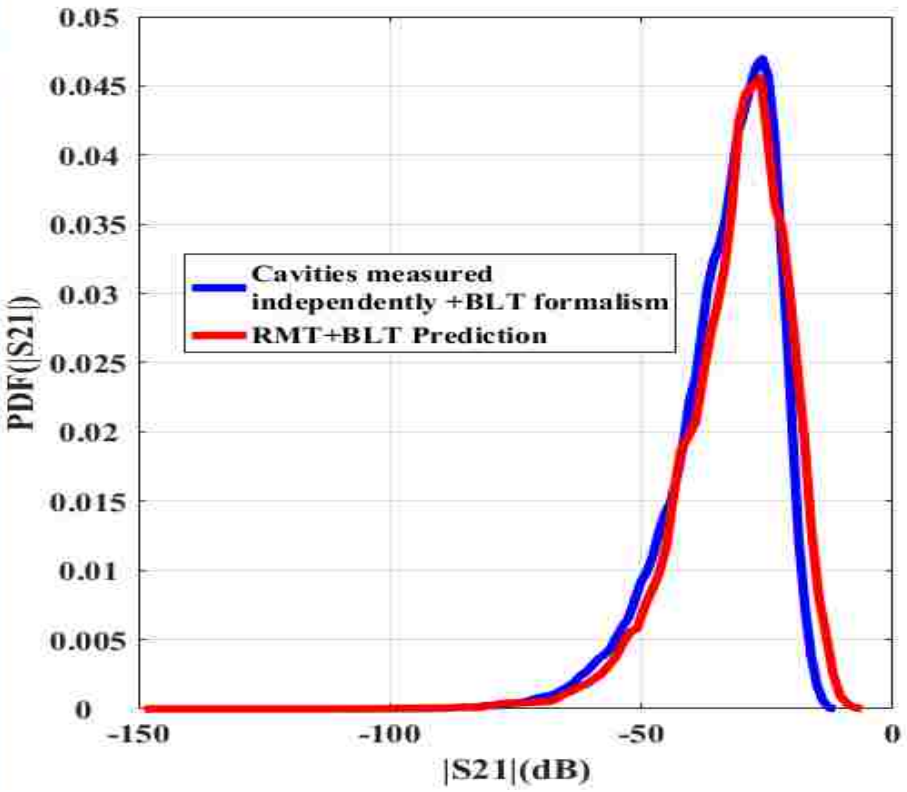

Fig. 3.9. BLT formalism results for two cascaded cavities.

Similarly, for three identical cascaded cavities, port 1 is connected to the antenna at location 3. Using a transmission line of 62" we connected the antenna at location 5 of the first cavity to the antenna at location 3 of the second cavity, and we connected the antenna at location 5 of the second cavity to the antenna at location 3 of the third cavity. The last cavity is connected to the PNA-X through antenna location 5.

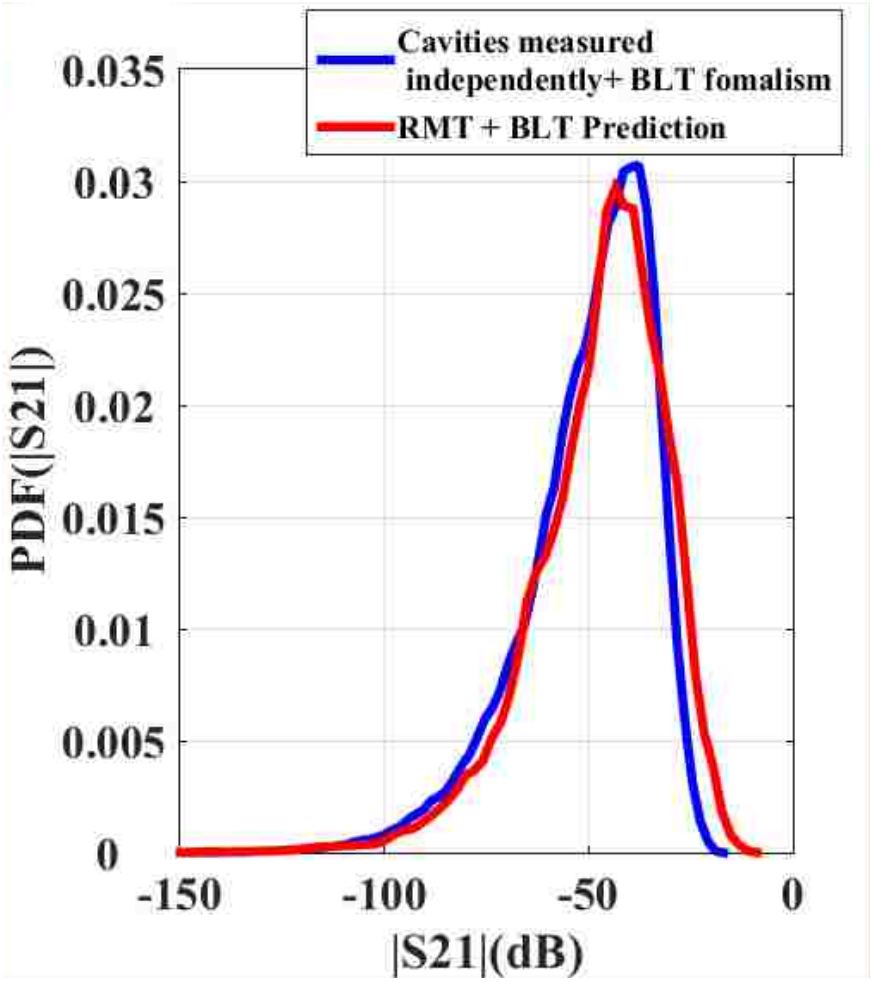

Fig. 3.10. BLT formalism results for three cascaded cavities.

A similar process is used for the setup with four and five cascaded cavities.

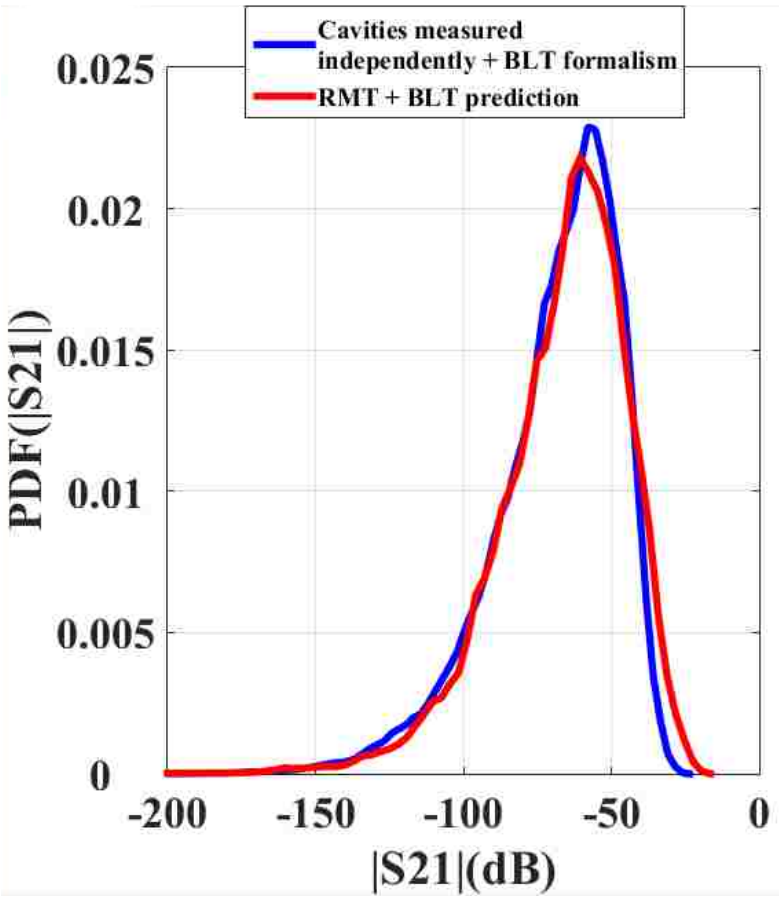

Fig. 3.11. BLT formalism results for four cascaded cavities.

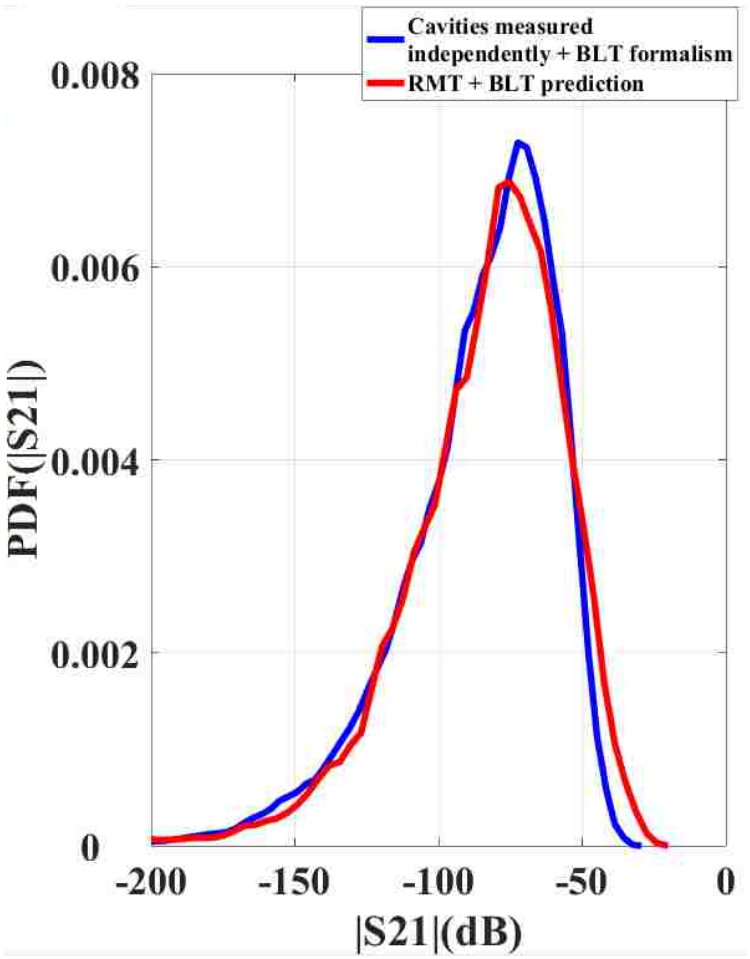

Fig. 3.12. BLT formalism results for five cascaded cavities.

Our results (Figs. 3.9-3.12) show an excellent agreement when fusing RCM with BLT for different networks of cascaded cavity configurations.

Chapter 4: Large 3D Cavity

In order to study the transition from deterministic to wave-chaotic behavior a large 3D chaotic cavity was designed and constructed. The 3D aluminum cavity (Fig. 4.1a) acts as a reverberation chamber with paddle-wheel blades. Fig. 4.1b shows the mode stirrer controlled by a LabVIEW program that rotates it incrementally in 200 steps. Each step in the rotation yields different electromagnetic field configurations (see Fig. 4.1c). The cavity is connected using two transmission lines that connect to a Keysight E5061B VNA. The cavity is driven by two coupled ports and is excited using two Hertzian dipole antennas to generate a large statistical ensemble of a 2x2 cavity scattering matrix $\overleftrightarrow{S}$.

To generate a very large ensemble of data, the electromagnetic configuration inside the cavity changes for each degree rotation as the mode stirrer is incrementally turned. At each increment $\overleftrightarrow{S}$ is measured as a function of frequency in 100 MHz increments from 300 MHz to 3 GHz; we chose this frequency range to enable us to study the transition from the deterministic to wave-chaotic regime. By rotating the mode stirrer in 200 steps, an ensemble of 320200 cavity scattering matrices is obtained at each 100 MHz increment. We use the method described in Chapter 2 to generate $\overleftrightarrow{S}$.

(a)

(b)

(c)

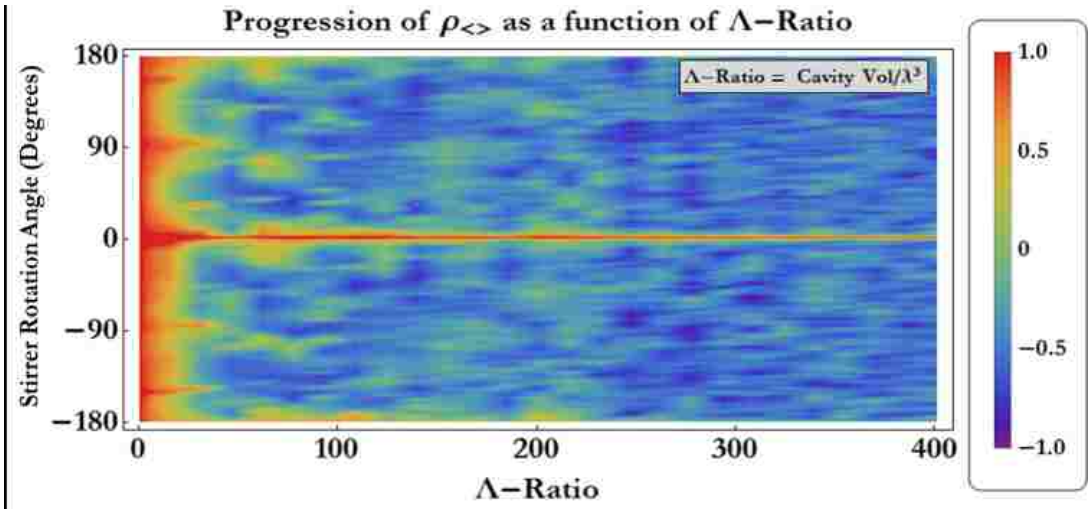

Fig. 4.1. (a) Photograph of the experimental setup of a single 3D aluminum cavity. (b) Photograph of the mode stirrer inside the cavity. (c) Plot of the correlation between one rendition of the cavity vs. other renditions of the cavity as the stirrer is rotated through 360 degrees.

4.1 Experimental Chaos Verification for a Single 3D Cavity

We verify the existence of wave-chaotic scattering in our 3D cavity in the high frequency limit by verifying the statistical independence of the phase and magnitude of the normalized eigenvalues of $\overleftrightarrow{S}$ (Dyson's circular ensemble hypothesis, previously described). Fig. 4.2 shows the polar contour density plot for $\{\mathrm{Re}[\lambda_s], \mathrm{Im}[\lambda_s]\}$ in the frequency range of 2.7-2.8 GHz where the loss parameter of the cavity is 1.6. Using Dyson's hypothesis, we confirm that our 3D aluminum cavity is chaotic above 1.6 GHz.

Fig. 4.3 presents the PDFs of the real and imaginary parts of the grouped eigenvalues of the normalized impedance matrix given the value of α=1.6 (loss parameter) obtained using experimental measurements. The results agree well with the simulation results from the RCM.

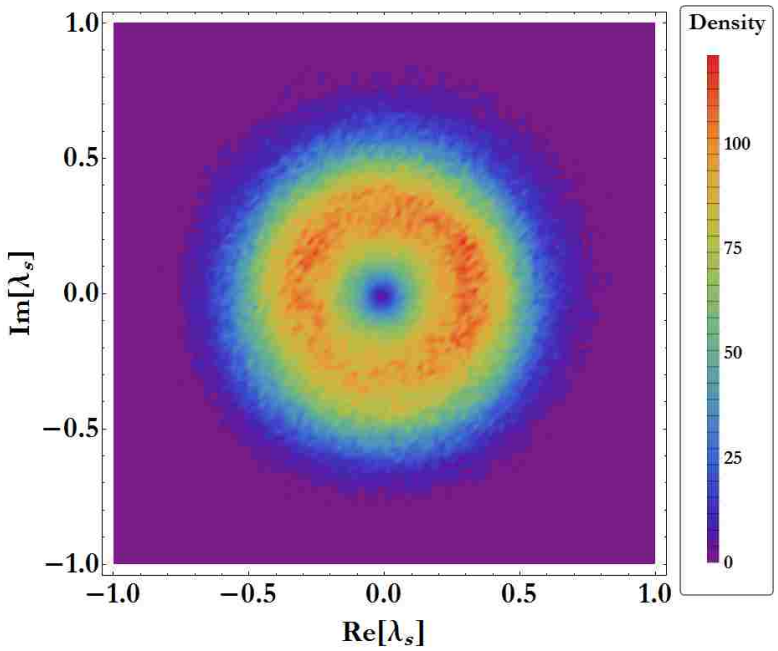

Fig. 4.2. Polar contour density plot of real λ_s vs. imaginary λ_s.

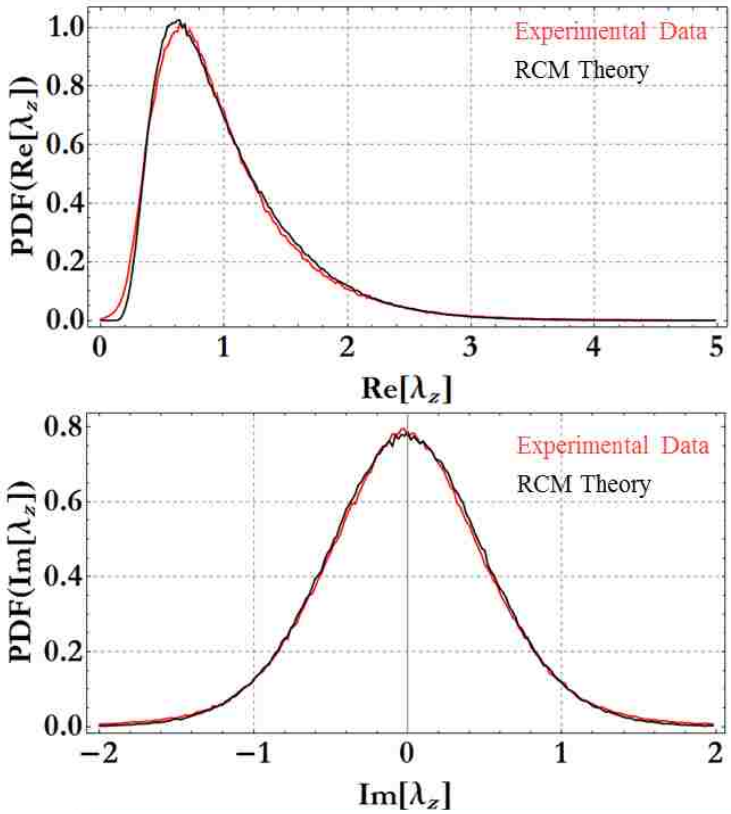

Fig. 4.3. Comparison of experimental data with results from the RCM.

4.2 3D MSC Experiments for Verification for Deterministic Solutions

Our aluminum 3D MSC is also extensively used to experimentally verify the deterministic solutions for induced electromagnetic fields inside a ray-chaotic enclosure. The 3D cavity has been experimentally used to validate the applicability of the hybrid formulation. The hybrid formulation is the combination of the RCM and CEM (Computational Electromagnetic Method). The goal of the first experiment was to obtain the impedance matrix using finite elements method (FEM) for two ports antenna subsystems at lower frequency 800-900 MHz to validate its applicability. Fig 4.4 shows the experimental data I obtained to validate the computed S_{11} and S_{12} parameters as a function of frequency.

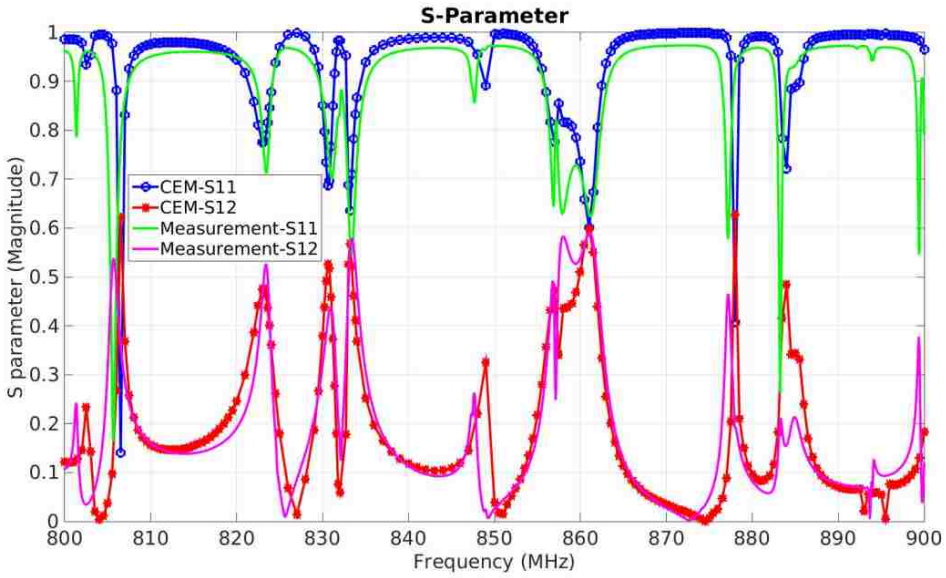

Fig. 4.4. Comparison of S-parameters obtained by computation and measurement.

Fig. 4.5 shows the S-parameters I measured using one port when the cavity is excited using an X-band waveguide in comparison with the deterministic computational methods obtained by Dr. Peng's group in the frequency range of 9-11 GHz.

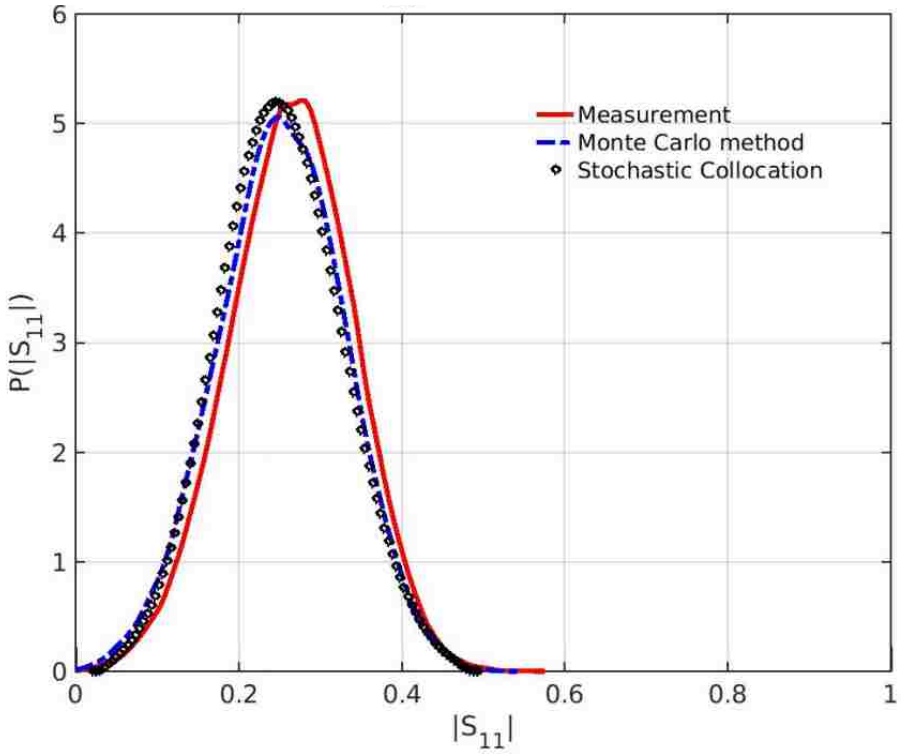

Fig. 4.5. PDF of $|S_{11}|$ in the single-port case.

The final results show an excellent agreement between measured and computed data.

Chapter 5: Conclusions and Scope for Future Work

We have created a platform that is a surrogate for a very large enclosure composed of volumes described by the BLT topology, and each volume is in accordance with the requirements for the RCM to be valid. We have verified that a statistical approach to solving a very large and complex electromagnetic problem can be achieved using the statistical models through verifying experimental and theoretical results for different network combinations. The combining of the RCM and the BLT electromagnetic topology provides the user with a quick tool to calculate the statistical distribution of the induced electromagnetic fields within large interconnected cavities. Using statistical approaches in solving large complicated problems is highly reliable, more rapid, and less expensive than performing a deterministic calculation of the problem.

This study also comes with few limitation controlled by the behavior of waves inside the ray-chaotic enclosures. In the low-frequency regime, all the cavities were not sufficiently chaotic where the RCM is applicable to produce statistical predictions. RCM is not applicable using hybrid systems which are the combination of chaotic, non-chaotic, and scarred modes. The RCM is also not applicable when we have an active circuitry with time-varying radiation impedances, and when there is a large multimode port which has variable radiation impedance that depends on the modes.

The STUWEE framework considers that every volume in the BLT network is ray-chaotic and statistical; therefore, any non-chaotic volume inside the BLT network will have to be accounted for using deterministic methods or as future work we can have a statistical method that accounts for non-chaotic enclosures.

5.1 Creating a STUWEE Simulation Software Tool

Simulation tools previously created to solve for the BLT topology, such as CRIPTE [10] and IDS Ingegneria Dei Sistemi [11], utilized deterministic solutions to the BLT nodes (which require detailed information on the interacting cavity volumes). This is where our proposed STUWEE code differs from them; we use a statistical treatment for the internal cavity fields based on the RCM. We are currently in the process of developing an engineering software tool that fuses the BLT electromagnetic topology model with the RCM to provide a fast calculation of the induced fields within a large a facility to rapidly assess a complex facility for vulnerability to electromagnetic attack. We plan on having an engineering software tool (STUWEE) fully developed in MATLAB and Qt.

Anticipated user inputs for the STUWEE code are:

- The number of cavities
- Loss parameter for each cavity
- The number of ports exciting each cavity.

Anticipated output for the STUWEE code:

- The induced currents and voltages within systems of interconnected and complicated enclosures.

5.2 RF and Microwave Effects on Digital Electronics

As future work, we want to study how the RCM fluctuations induced within a cavity can affect digital electronics inside ray-chaotic enclosures. Ultimately characterizing and understanding the microcontroller port impedance behavior as a function of instruction will allow us to implement a correction factor for this effect. This, in turn, will enable us to utilize these devices in irradiating wave-chaotic cavities and to accurately measure the coupling and ultimately the

effects of electromagnetic energy that will lead to a full back box predictive mode of electromagnetic interference effects.

5.3 Formulating a Time Domain Version of the Random Coupling Model

We are currently performing time domain experiments of multi-path reflections using quasi-2D cascaded cavities to test for the wireless communication response research that is being performed in the City of Albuquerque. The emulation of realistic wireless channels is performed through irregular cavities with high losses [9]. The cavity eigenspectrum can be generated using the universal statistical laws of RMT.

5.4 Formalism of BLT Using a Microwave Circulator

We will be constructing a network of a different type to further validate the success of the RCM/BLT formalism. We first measure the S-parameter of one quasi-2D cavity with no inserts when it is excited by four ports. Port 1 of the PNA-X will be connected to the antenna at location 3, port 2 will be connected to the antenna that will be connected to the antenna at location 4, port 3 will be connected at location 2, and port 4 will be connected to the antenna at location 1; we verify that the cavity is wave-chaotic. Once we confirm the existence of chaotic rays inside a cavity excited by four ports, we move to our first experiment. The test setup for the first network, Fig. 5.1, will have the antenna at location 2 connected through a 60” long coaxial transmission line to the antenna at location 1, rather than port 3 and port 4 respectively with no circulator. Its topological network is shown in Fig. 5.2. In this case, all five mode stirrers of the cavity are rotating at the same time for 200 times, and we measure complex S-parameter as a function of frequency per rotation.

For the second experiment, we repeat the same process as in the first experiment; however, the antenna at location 2 will connect to port 1 of a circulator through a 32” long transmission line,

and antenna at location 1 will connect to port 2 of the circulator through a 32” long transmission line, Fig. 5.3; in this case, the circulator ferromagnetic device is going to regulate the signal flow within the cavity. In the second experiment, the wave that enters port 1 of the circulator is going to be transmitted through port 2 into the cavity. The circulator provides one path in which the waves can travel. This is in contrast with experiment 1 where there was no circulator to regulate the waves. Fig. 5.4 shows that the waves, as explained in the BLT topological network, are traveling back and forth into and out of the cavity through the transmission line.

As we have tested before, all our quasi-2D cavities obey Time Reversal Symmetry (TRS); therefore, we use the Gaussian Orthogonal Ensemble (GOE) of the random matrices to test the measurement of our experiments vs. the BLT electromagnetic topology model with the RCM prediction.

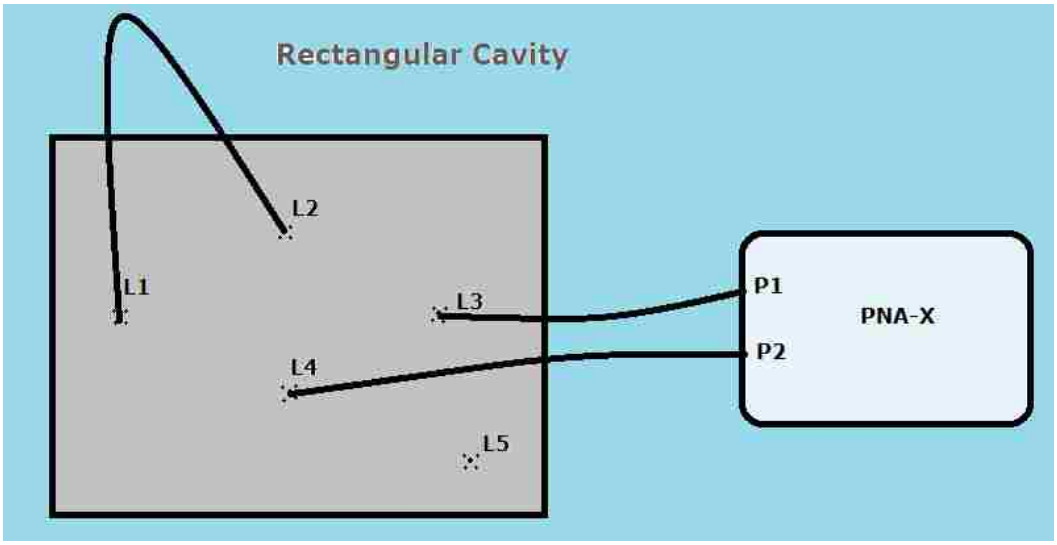

Fig. 5.1. Schematic of our experimental setup for a network with no circulator.

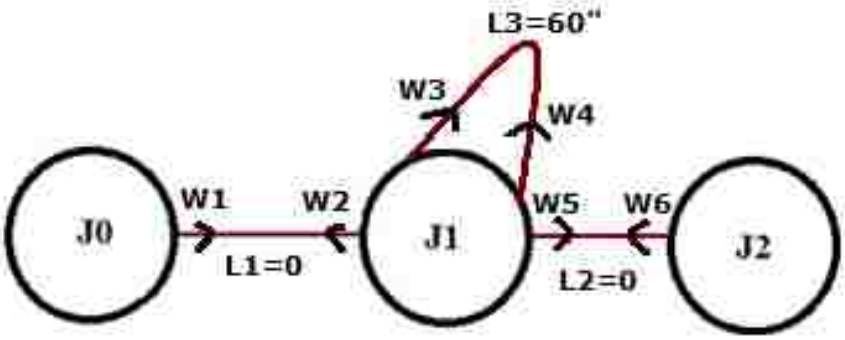

Fig. 5.2. BLT topological network with no circulator.

$$\overleftrightarrow{S} = \begin{pmatrix} 0 & 0 & 0 & 0 & 0 & 0 \\ S11 & 0 & 0 & S14 & 0 & 0 \\ S31 & 0 & 0 & S34 & 0 & 0 \\ 0 & 0 & S43 & 0 & 0 & S42 \\ 0 & 0 & S23 & 0 & 0 & S22 \\ 0 & 0 & 0 & 0 & 0 & 0 \end{pmatrix}, \text{ and} \tag{5.1}$$

$$\overleftrightarrow{F} = \begin{pmatrix} 1 & 0 & 0 & 0 & 0 & 0 \\ 0 & 1 & 0 & 0 & 0 & 0 \\ 0 & 0 & e^{-j\frac{2\pi f}{c}*L1} & 0 & 0 & 0 \\ 0 & 0 & 0 & e^{-j\frac{2\pi f}{c}*L1} & 0 & 0 \\ 0 & 0 & 0 & 0 & 1 & 0 \\ 0 & 0 & 0 & 0 & 0 & 1 \end{pmatrix}. \tag{5.2}$$

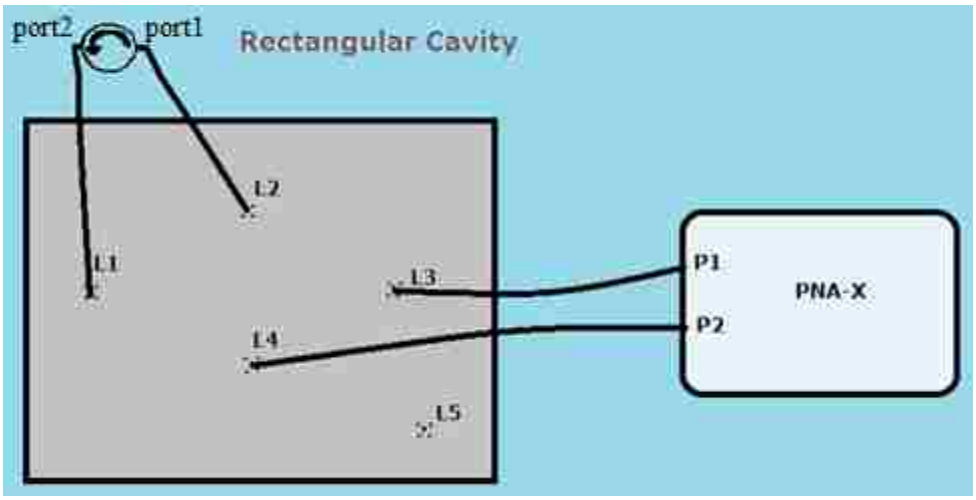

Fig. 5.3. Schematic of experimental setup for a network with no circulator.

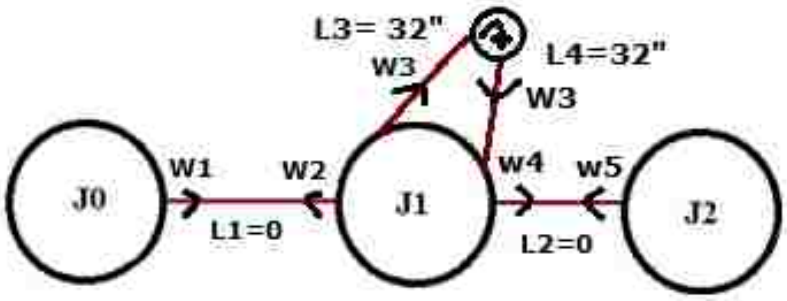

Fig. 5.4. BLT topological network for a network with a circulator.

$$\overleftrightarrow{S} = \begin{pmatrix} 0 & 0 & 0 & 0 & 0 \\ S11 & 0 & 0 & 0 & 0 \\ S31 & 0 & 0 & 0 & S32 \\ 0 & 0 & S23 & 0 & S22 \\ 0 & 0 & 0 & 0 & 0 \end{pmatrix}, \text{ and} \tag{5.3}$$

$$\overleftrightarrow{\Gamma} = \begin{pmatrix} 1 & 0 & 0 & 0 & 0 \\ 0 & 1 & 0 & 0 & 0 \\ 0 & 0 & e^{-j\frac{2\pi f}{c}*L3} & 0 & 0 \\ 0 & 0 & 0 & e^{-j\frac{2\pi f}{c}*L4} & 0 \\ 0 & 0 & 0 & 0 & 1 \end{pmatrix}. \tag{5.4}$$

5.5 Data-Driven Discovery of Electromagnetic Topology

We are using the five quasi-2D cavities to experimentally validate the solutions obtained deterministically by Dr. Peng's group at the University of New Mexico. The goal is to discover the topological graph of electromagnetic systems based on data collected in experiments and simulations. Key ingredients include a sparse, nonlinear regression to determine the interaction channels between graph nodes, and a recursive skeletonization factorization for the dimensionality reduction of large datasets. An example of Dr. Peng's data-driven discovery of electromagnetic topology vs. our measurements shows an almost perfect agreement, Fig. 5.5.

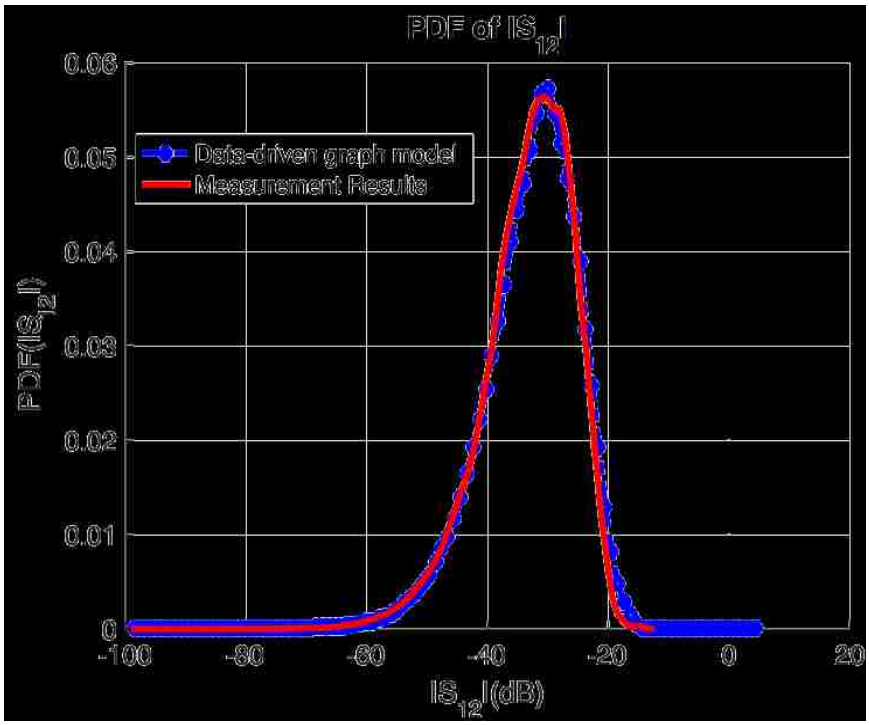

Fig. 5.5. Data-driven discovery of electromagnetic topology (blue) vs. measurements (red).

Predicting the statistical nature of short wavelength reverberation within random interconnections of large and complicated cavities finds applications in several fields of physics

and engineering. In this Dissertation, we have proved the validity of solving complex electromagnetic problems in a concise amount of time using two types of successful wave scattering models, the RCM and BLT electromagnetic topology model, that describes the interaction of short wavelength electromagnetic radiation within complicated enclosures, and the interaction of interconnected networks of large and complicated enclosures.

5.6 Additional Reading

In addition to the references cited in this Dissertation I have provided references to additional reading that might guide future research [12-25].

References

[1] S. Hemmady, A Wave-Chaotic Approach to Predicting and Measuring Electromagnetic Field Quantities in Complicated Enclosures, (Ph.D. Thesis, University of Maryland, College Park, MD, 2006).

[2] J.P. Parmantier, "Numerical Coupling Models for Complex systems and Results," IEEE Trans. Electromag. Compat., vol. 46, 359 (2004), and references therein.

[3] X. Zheng, T.M. Antonsen and E. Ott, "Statistics of Impedance and Scattering Matrices in Chaotic Microwave Cavities: Single Channel Case," Electromagnetics, vol. 26, pp. 3-35 (2006).

[4] X. Zheng, T.M. Antonsen and E. Ott, "Statistics of Impedance and Scattering Matrices of Chaotic Microwave Cavities with Multiple Ports," Electromagnetics, vol. 26, pp. 37-55 (2006).

[5] H.-J. Stoackmann, Quantum Chaos (Cambridge University Press, Cambridge, UK, 1999).

[6] C.E. Baum, "Electromagnetic Topology: A Formal Approach to the Analysis and Design of Complex Electronic Systems," Interaction Note 400 (http://ece-research.unm.edu/summa/notes/In/0400.pdf) (1980).

[7] G. Gradoni, J.-H. Yeh, B. Xiao, T.M. Antonsen, S.M. Anlage, and E. Ott, "Predicting the Statistics of Wave Transport through Chaotic Cavities by the Random Coupling Model: A Review and Recent Progress," Wave Chaos, vol. 51, 606 (2014).

[8] J.P. Parmantier, J.C. Alliot, G. Labaune, and P. Degauqe, "Electromagnetic Coupling on Complex Systems: Topological Approach," Interaction Note 488 (http://ece-research.unm.edu/summa/notes/In/0488.pdf) (1990).

[9] G. Gradoni, X. Chen, T.M. Antonsen, S.M. Anlage, and E. Ott, "Random Coupling Model

for Wireless Communication Channels," *Proc. 2014 International Symposium on Electromagnetic Compatibility (EMC Europe)* (Gothenburg, Sweden, Sept. 1-4, 2014) pp. 878-882 (2014).

[10] J.P. Parmantier and S. Bertuol, "CRIPTE: User Guide," S.l.: ONERA/DEMR -009/06 – S, (2006), vol. CRIPTE 4.2.

[11] IDS Ingegneria Dei Sistemi, https://www.idscorporation.com/naval/our-solutions-services/emc-emi-prediction-measurement.html

[12] X. Li, C. Meng, Y. Liu, E. Schamiloglu, and S. Hemmady, "Experimental Verification of a Stochastic Topology Approach for High-Power Microwave Effects," IEEE Trans. Electromagn. Compat., vol. 57, pp. 448-453 (2015).

[13] S. Hemmady, X. Zheng, T.M. Antonsen, E. Ott, S.M. Anlage, "Universal Properties of 2-Port Scattering, Impedance and Admittance Matrices of Wave Chaotic Systems," Phys. Rev. E, vol. 74, 036213 (2006).

[14] J.P. Parmantier and I. Junqua, "EM Topology: From Theory to Application," in Ultra-Wideband, Short-Pulse Electromagnetics 7 (Springer, New York, NY, 2007), pp. 3-12.

[15] J.P. Parmantier, X. Ferrieres, S. Bertuol, and C.E. Baum, "Various Ways to Think of the Resolution of the BLT Equation with an LU Technique," Interaction Note 535 (http://ece-research.unm.edu/summa/notes/In/0535.pdf) (1998).

[16] C.E. Baum, T.K. Liu, and F.M. Tesche, "On the Analysis of General Multiconductor Transmission Line Networks,' Interaction Note 350 (http://ece-research.unm.edu/summa/notes/In/0350.pdf) (1978).

[17] K.S.H. Lee, EMP Interaction: Principles, Techniques, and Reference Data: A Handbook of Technology from The EMP Interaction Notes (Hemisphere Publishing, New York, NY, 1986).

[18] J.P. Parmantier, V. Gobin, F. Issac, I. Junqua, Y. Daudy, and J.M. Lagarde, "An Application of the Electromagnetic Topology Theory on the Test- Bed aircraft, EMPTAC," Interaction Note 506 (http://ece-research.unm.edu/summa/notes/In/0506.pdf) (1993).

[19] G. Bedrosian and K.S.H. Lee, EMP Penetration Through Metal Skin Panels and Into Aircraft Cavities, Interaction Note 315 (http://ece-research.unm.edu/summa/notes/In/0314.pdf) (1976).

[20] J.P. Parmantier and P. Degauque, "Topology Based Modeling of Very Large Systems," Modern Radio Science, J. Hamelin (Ed.) (Oxford University Press, Oxford, UK, 1996), pp. 151-177.

[21] J.P. Parmantier, V. Gobin, F. Issac, I. Junqua, Y. Daudy, and J.M. Lagarde, "ETE 3: Application of the Electromagnetic Topology Theory on the EMPTAC," Interaction Note 527 (http://ece-research.unm.edu/summa/notes/In/0527.pdf) (1997).

[22] F.M. Tesche, M.V. Ianoz, and T. Karlsson, EMC Analysis Methods and Computational Models, (John Wiley and Sons, New York, NY, 1997).

[23] J.P. Parmantier, "An Efficient Technique to Calculate Ideal Junction Scattering Parameters in Multiconductor Transmission Line Networks," Interaction Note 536 (http://ece-research.unm.edu/summa/notes/In/0536.pdf) (1998).

[24] M. Abrams, "Dawn of the E-bomb," IEEE Spectrum (2013).

[25] "Electromagnetic Pulse," Wikipedia, The Free Encyclopedia, accessed 13 June 2017, https://en.wikipedia.org/wiki/Electromagnetic_pulse.